

When do bursts matter in the primary motor cortex? Investigating changes in the intermittencies of beta rhythms associated with movement states

Timothy O. West^{a,b,*}, Benoit Duchet^a, Simon F. Farmer^{c,d}, Karl J. Friston^b, Hayriye Cagnan^{a,b}

^a Medical Research Council Brain Network Dynamics Unit, Nuffield Department of Clinical Neurosciences, University of Oxford, Mansfield Road, Oxford OX1 3TH, UK

^b Wellcome Centre for Human Neuroimaging, Queen Square Institute of Neurology, University College London, London WC1N 3BG, UK

^c Department of Neurology, National Hospital for Neurology & Neurosurgery, Queen Square, London WC1N 3BG, UK

^d Department of Clinical and Movement Neurosciences, UCL Institute of Neurology, Queen Square, London WC1N 3BG, UK

ARTICLE INFO

Keywords:

Neural activity
Movement control
Cortex
Bursts
Simulation
Brain circuits
Primary motor cortex

ABSTRACT

Brain activity exhibits significant temporal structure that is not well captured in the power spectrum. Recently, attention has shifted to characterising the properties of intermittencies in rhythmic neural activity (i.e. bursts), yet the mechanisms that regulate them are unknown. Here, we present evidence from electrocorticography recordings made over the motor cortex to show that the statistics of bursts, such as duration or amplitude, in the beta frequency (14–30 Hz) band, significantly aid the classification of motor states such as rest, movement preparation, execution, and imagery. These features reflect nonlinearities not detectable in the power spectrum, with states increasing in nonlinearity from movement execution to preparation to rest. Further, we show using a computational model of the cortical microcircuit, constrained to account for burst features, that modulations of laminar specific inhibitory interneurons are responsible for the temporal organisation of activity. Finally, we show that the temporal characteristics of spontaneous activity can be used to infer the balance of cortical integration between incoming sensory information and endogenous activity. Critically, we contribute to the understanding of how transient brain rhythms may underwrite cortical processing, which in turn, could inform novel approaches for brain state classification, and modulation with novel brain-computer interfaces.

1. Introduction

Rhythmic activity from populations of neurons, as is routinely summarised using the power spectrum, is often leveraged to characterise neural activity from different brain regions (Keitel and Gross, 2016; Mahjoory et al., 2020), behavioural states (Siegel et al., 2012), and pathologies (Brown et al., 2001; Schnitzler and Gross, 2005). However, when analysed in time, neural rhythms often resolve into a succession of intermittent, transient events (Baker et al., 2014; van Ede et al., 2018; Feingold et al., 2015; Fingelkurts and Fingelkurts, 2010; Freeman, 2004; Friston, 1997) that can appear as sustained oscillations when investigated using trial averaged analyses (van Ede et al., 2018; Jones, 2016). To understand how alterations in power are underwritten by the temporal restructuring of neural rhythms, it is necessary to explicitly quantify the duration, amplitude, and rate of transient events (Heide- man et al., 2020).

Temporal intermittencies in neural rhythms (i.e., “bursts”) are

known to be important in behaviours such as sleep (Adamantidis et al., 2019) and working memory (Lundqvist et al., 2016). In the healthy motor system, changes in the temporal organisation of beta frequency (14–30 Hz) activity can predict behaviour beyond that achieved when using just the amplitude of beta activity (Enz et al., 2021; Hannah et al., 2020; Shin et al., 2017; Wessel, 2020). Further, beta burst dynamics appear to be significantly altered in Parkinsonism (Cagnan et al., 2019; Deffains et al., 2018; Tinkhauser et al., 2017b), where they form a major target for adaptive deep brain stimulation (Little et al., 2016; Tinkhauser et al., 2017a). Properties of transient activity can, in principle, improve the accuracy of brain state classification and thus have the potential to inform stimulation controllers that are adaptive to changes in behavioural context.

In the context of motor behaviour, preparation and execution have been described in terms of event-related synchronisation and desynchronisation in the beta frequency band (Pfurtscheller and Lopes da Silva, 1999). Movement imagery has also been linked to event-related

* Corresponding author at: Medical Research Council Brain Network Dynamics Unit, Nuffield Department of Clinical Neurosciences, University of Oxford, Mansfield Road, Oxford OX1 3TH, UK.

E-mail address: timothy.west@ndcn.ox.ac.uk (T.O. West).

<https://doi.org/10.1016/j.pneurobio.2022.102397>

Received 29 July 2022; Received in revised form 4 November 2022; Accepted 19 December 2022

Available online 21 December 2022

0301-0082/© 2022 The Authors. Published by Elsevier Ltd. This is an open access article under the CC BY license (<http://creativecommons.org/licenses/by/4.0/>).

desynchronisation albeit with less power decrease at beta frequencies than that seen during movement execution (Pfurtscheller and Neuper, 1997). When beta frequency activity is temporally resolved, changes in the rate and timing of bursts are associated with movement preparation, planning, termination or cancellation (Diesburg et al., 2021; Feingold et al., 2015; Khanna and Carmena, 2017; Little et al., 2019; Torrecillos et al., 2018; Tzagarakis et al., 2010; Wessel, 2020). Additionally, beta bursts are associated with effects that persist beyond their termination (Khanna and Carmena, 2017; Torrecillos et al., 2018). Recent evidence also suggests that bursts reflect a competition between endogenous processing and external sensory responses that can bias perception in the cortex (Karvat et al., 2021).

Taken together, we hypothesise that: (1) the temporal properties of beta bursts are altered between different movement states such as rest, movement preparation, movement execution, and movement imagery; (2) these changes in temporal organisation reflect altered responses of the motor cortex to stochastic inputs, that arise from a reconfiguration of the underlying microcircuit, and thus, (3) that expression of bursts reflect a rebalancing of how the cortex integrates spontaneous and exogenous inputs.

To date, the mechanisms underlying burst activity have been described using relatively simple models, such as an excitatory/inhibitory network of Wilson-Cowan populations (Duchet et al., 2021; Powanwe and Longtin, 2019; Xing et al., 2012) that are motivated by pyramidal-interneuron models of beta generation (Jensen et al., 2005; Kopell et al., 2011). These studies indicate that burst statistics are determined by interactions between synaptic noise and the connectivity parameters of any given model. This suggests that models constrained using burst statistics can more accurately infer underlying connectivity across states. In more structurally fine-grained models, work has demonstrated the importance of laminar-specific corticothalamic inputs, which given the right timing can generate short, high amplitude beta events in the absence of endogenous neural activity (Sherman et al., 2016). Whilst these models have been useful in understanding how to either experimentally or therapeutically modulate the mechanisms that give rise to beta bursts, it is still not known how changes in burst statistics between brain states may be underwritten by alterations in laminar specific excitability, and how spontaneous rhythmic activity interacts with exogenous inputs to the cortex.

Here, we aim to establish how alterations in the cortical microcircuitry manifest in the burst statistics of beta rhythms recorded from large scale neuronal activity. To this end, we use a library of publicly available electrocorticography (ECoG) data recorded from participants performing a range of motor tasks (Miller, 2019). We first investigated how rhythmic burst features in these data may enhance the classification of different motor stages – such as movement preparation, execution, and imagery – by providing information beyond that available in the time-averaged spectra. Secondly, using computational models of the motor cortex microcircuit constrained to explain both the power spectra and bursting properties of the ECoG data, we characterise how biophysical parameters may modulate bursting dynamics in different brain states. Finally, we use this model to test the hypothesis that changes in spontaneous cortical activity can reflect an altered balance in how the cortex integrates endogenous and exogenous inputs.

2. Methods

2.1. Electrocorticography and experimental recordings

All experimental data were taken from an openly available library (Miller, 2019) that are published for use without restriction (<https://se-archworks.stanford.edu/view/zk881ps0522>). Recordings were made for anatomical mapping in patients with epilepsy at Harborview Hospital, Seattle, WA, USA. All patients provided informed written consent, under experimental protocols approved by the Institutional Review Board of the University of Washington (see supplementary information

VII). Data were recorded at the bedside using Synamps2 amplifiers (Compumedics Neuroscan). Visual stimuli were presented using a monitor running BCI2000 stimulus and acquisition programmes (Schalk et al., 2004). Electrocorticography (ECoG) was recorded using grids and/or strips of platinum subdural electrodes placed via craniotomy. Electrodes had a 4 mm diameter (2.3 mm exposed) with 1 cm inter-electrode distance and were embedded in silastic. Electrical potentials were recorded at 1 KHz using a scalp/mastoid reference and ground. Hardware imposed a bandpass filter from 0.15 to 200 Hz. Locations of electrodes were confirmed using post-operative radiography. Exact details of the electrode localisation methods can be found in Miller (2019).

Data were taken from three different tasks as summarised below. For details of task structure and trial definitions please see Fig. 1A. Subject numbers represent the initial total available for each task, some subjects participated in more than one task. Data selection procedures are outlined in Section 2.2.

Dataset 1: Self-Paced Finger Movements ($n = 9$) – originally reported in Miller et al. (2012). Participants were cued with a word displayed on a bedside monitor indicating which digit to perform a self-paced flexion and extension during a 2 s movement trial. Trials typically comprised 2–5 movements as recorded using a data glove. Movement blocks were interleaved with 2 s rest trials. Data were taken from the “fingerflex” folder of the Miller repository.

Dataset 2: Basic Motor ($n = 19$) – originally reported in Miller et al. (2007) and Miller et al. (2010). Participants were asked to make either a simple repetitive flexion and extension of all the fingers, or a protrusion and retraction of the tongue at a self-paced rate (~2 Hz). Patients were cued with a picture of the body part to move, presented on a screen. Data were taken from the “motor_basic” and “imagery_basic” folders of the Miller repository.

Dataset 3: Motor Imagery ($n = 7$) – originally reported in Miller et al. (2010). Participants were asked to imagine making a simple repetitive flexion and extension of the fingers, or protrusion/protraction of the tongue at a self-paced rate (~2 Hz), matched to the task described for dataset 2. Imagery was intended to be kinaesthetic rather than visual- i.e., “imagine making the motion, not what it looked like”. Movement blocks lasted 2 or 3 s and were always followed by rest intervals of the same length. Data were taken from the “imagery_basic” folder of the Miller repository.

2.2. Pre-processing and criteria for data selection

All ECoG recordings were processed as summarised in Fig. 1B. Large scale artefacts common across sensors were reduced by referencing electrodes to the common average. Channels with significant artefacts or epileptiform activity were rejected visually and excluded from the common average. Data were filtered between 4 and 98 Hz using a zero-phase (i.e., forward-backwards) FIR filter with – 60 dB stopband attenuation. As the calculations of beta band signal-to-noise ratio (SNR) involved a comparison with the mean amplitude of the background, we chose a high-pass filter with a 4 Hz cut-off frequency to reduce the influence of 1/f increase in amplitude at low frequencies.

For each set of recordings, we selected one ECoG channel to carry forward for analysis. Data were selected to identify signals which were relevant to motor activity (i.e., spatially close to the primary motor cortex), of sufficient quality (i.e., good SNR of beta frequency activity), and functionally relevant (i.e., showing task related changes in synchrony). An illustration of the selection process can be seen in Fig. 1C. Channels were selected based on the following criteria: (1) select channels within 30 mm of left or right primary motor cortex (MNI: $[-37 -25 62]$; Jha et al., 2015); (2) threshold channels at + 5 dB SNR for the beta band (14–30 Hz); (3) select a channel based on maximum SNR change between rest and movement/imagery. If no channels were found that matched these criteria the subject was removed from further analysis. The number of subjects whose data was carried forward for further analysis was: 5/9 subjects from dataset 1; 10/19 subjects from

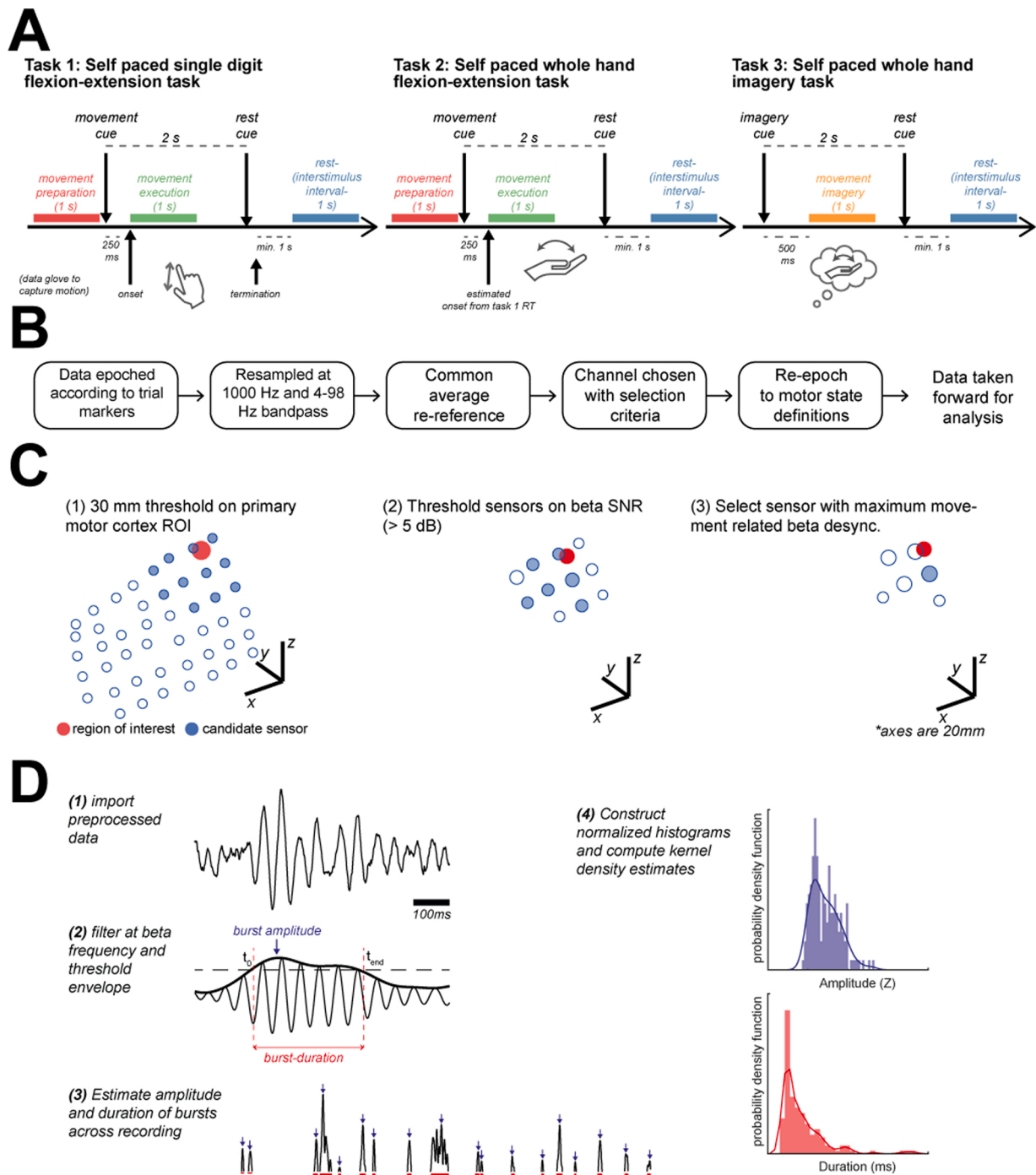


Fig. 1. Illustrated criteria for selection of ECoG channels and computed data features: spectra, and distributions of burst amplitudes and durations. (A) Data were taken from three motor tasks, requiring either self-paced flexion/extension of individual digits (task 1); or flexion/extension of the whole hand (task 2); or imagery of a whole hand movement (task 3). Data were epoched according to timings relative to those given in the figure. (B) Procedures for preprocessing data. (C) Illustration of channel selection procedure. Candidate ECoG channels (blue open circles) were selected (filled blue circles) using a 30 mm search radius of the ROI (MNI coordinate: $[-37 -25 62]$; red circle). All channels were thresholded at a + 5 dB SNR level for the beta peak (see methods), finally channels were selected using the maximum movement related beta desynchronisation. (D) Illustration of the envelope threshold procedure to identify bursts. Samples of burst amplitudes and durations were used to construct histograms. Summaries of these distributions were then taken as the kernel estimate of the probability density function.

dataset 2; and 4/7 from dataset 3.

Only one channel per subject was selected for the full analysis. This is because the number of channels that passed the selection criteria was variable across subjects, and pooling between neighbouring sensors had the potential to bias the construction of burst distributions due to the superposition of multiple underlying cortical sources. This is supported by distributions of spectral and burst features computed in an example

subject (supplementary methods VI; [Supplementary Fig. 7](#)), that show that there is a spatial spread of burst features across multiple sensors ([Zich et al., 2020](#)).

Data from each task were segmented into 1 s epochs. Details of epoching are illustrated in [Fig. 1A](#). For dataset (1), kinematic data was available from a data glove worn during the experiment, and thus data was epoched according to movement onset (finger movements)

determined using a threshold crossing on the smoothed movement traces. Data was segmented into *movement preparation* (−1250 ms to −250 ms relative to movement onset) and *movement execution* (0 ms to +1000 ms relative to movement onset) and then 1 s *interstimulus interval* (ISI) blocks taken in between movement cues. ISI blocks were always at least 1 s away from a movement cue or movement termination. Throughout this paper we denote data from ISI blocks as “Rest”. Note that we left a 250 ms gap prior to movement onset to avoid non-stationarities that occur when beta exhibits movement related desynchronisation. This ensures that data arise from clearly defined states, rather than potentially containing data describing the transition between states. For datasets 2 and 3, movement kinematics were not available, and movement or imagination was cued by on-screen instructions. We therefore estimated movement onset using reaction times from dataset 1. If a subject also participated in dataset 1, we used their median subject-specific reaction time. For all other subjects, we used the group median from dataset 1. We took blocks of *movement execution* and *movement imagery* starting at cue onset plus this reaction time (lasting for 1 s in total). Movement preparation was defined as before.

2.3. Data features: Spectra and distributions of burst amplitude/duration

Time series data were summarised using features derived from both spectra and bursts. We computed power spectral densities using Welch's periodogram method with no overlap and a 1 s Hann window. Spectral features comprise the peak frequency within the beta band (14–30 Hz), wide-band SNR, and narrow-band SNR within the beta band (see supplementary methods I).

Bursts were defined using a threshold (75th percentile) on the bandlimited envelope (Cagnan et al., 2019; Tinkhauser et al., 2017b). Note that thresholds were specific to each condition (i.e., over the concatenated epochs from data in each movement state). This was performed to avoid the bias towards burst effects reflecting simple differences in SNR that can occur with a common threshold (Schmidt et al., 2020). This does however mean that burst properties are relative to the condition specific signal power, with the threshold for burst identification in movement execution, being systematically lower than that for movement preparation due to the difference in beta power between these conditions.

For an illustration of burst definitions and the formation of summary statistics of burst properties, see Fig. 1D. Briefly, the distributions of burst amplitude or duration for each recording are summarised in terms of a probability density of an arbitrary form (i.e., a kernel density estimate) which may be further reduced to its mean and standard deviation. Details of the procedure are given in supplementary methods III.

Overall, spectral features comprised: (1) wide-band SNR, (2) narrow-band SNR, and (3) peak frequency. Burst features comprised: (4) mean and (5) standard deviation of burst duration; (6) mean and (7) standard deviation of burst amplitude. Statistical tests of burst features were computed on log transformed data. For all features except peak frequency, a one-way ANOVA and post-hoc t-tests were used to test for changes in means of features between motor states. The distribution of peak frequencies was not found to be normal, therefore, a Kruskal-Wallis test plus post-hoc rank-sum tests were used to determine changes in mean.

Note that analyses of differences in signal recorded between motor states (results Section 3.1) use the above quantitative summaries of the data features (i.e., the seven features described above), whereas the model fitting procedures (results Section 3.3) utilises the full continuous data features (i.e., spectral density, and probability densities for bursts) to constrain model parameters.

2.4. Assessing feature nonlinearity: Comparison with linear surrogate data

To assess the extent to which statistics of burst features in cortical

signals encode information beyond that contained in the power spectrum, we used a comparison with surrogate data (Theiler et al., 1992). Following work characterising the degree of nonlinearity in beta bursts (Duchet et al., 2021), we use Iterative Amplitude-Adjusted Fourier Transforms (IAAFT; Schreiber and Schmitz, 1996). The IAAFT surrogate method improves upon the simpler technique of constructing randomised-phase Fourier surrogates, by not only ensuring the power spectrum is preserved, but also that the signal's probability density is preserved. This ensures that the surrogate reproduces the linear features of the data whilst destroying potential nonlinearities in the original time series. To compare data with IAAFT surrogates, we constructed 25 surrogate time series for each data set, and then took the feature average, computed in the same way as for the reference (i.e., the empirical or simulated) signals. We then computed the goodness-of-fit in terms of the R^2 , with $R^2 < 1$ indicating significant deviation of a data feature from that expected in the equivalent linear process.

2.5. Classification of functional states with a support vector machine

To determine the ability of different data features to decode the functional state from neural activity, we employed a classification approach. Prior to classification, we applied Linear Discriminant Analysis (LDA) to the data to reduce the dimensionality of the feature space to two LDA components. We then used a multiclass support vector machine (SVM) using error-correcting output codes to combine binary classifiers into an ensemble and applied this to the LDA feature space. Learners were implemented in MATLAB using iteratively optimised hyperparameters, and a Gaussian kernel set. Model performance was evaluated using five-fold cross validation and the area under the curve (AUC) of receiver operating characteristics (ROCs) across the folds. Plots of SVM decision bounds were computed using posterior probabilities of model predictions applied in a grid search across the feature space. In effect, these measures of classification accuracy constitute an empirical estimate of model evidence or marginal likelihood, where the model in question maps from a functional motor state to various data features.

2.6. Identification and fitting a model of motor cortex population activity

We used a neural mass model of population activity in the motor cortex microcircuit (i.e., Bhatt et al., 2016) that incorporates a middle layer reflecting the presence of layer 4 cells in primary motor cortex (Yamawaki et al., 2014). This neural (state space) model formulation follows from the Wilson-Cowan population firing rate model (Vogels et al., 2005; Wilson and Cowan, 1972). This model was first employed to describe the behaviour of large scale, aggregate, neural population activity such as thalamocortical oscillations (Wilson and Cowan, 1973) and since has been used extensively to explain cortical and subcortical rhythms (Deco et al., 2009; Lea-Carnall et al., 2016; Oswal et al., 2021; Pavlides et al., 2015; Powanwe and Longtin, 2019; Yousif et al., 2017). As a prelude to the current modelling, we compared the evidence for convolution models – specifically, extended Jansen and Rit-like models (Jansen and Rit, 1995) – against the simpler Wilson-Cowan like model. The Bayesian model comparison is detailed in supplementary methods V and Supplementary Fig. 4. Supplementary fig. 4 shows that the Wilson-Cowan formulation better fits the burst features as indicated by the superior model evidence. Unlike the Wilson-Cowan model, we also found that the Jansen-Rit model was not able to capture altered burst properties, reflecting motor state dependent changes – a critical component of our study. For these reasons we used the Wilson-Cowan formulation in the remainder of this work.

The states of the Wilson-Cowan model depict *instantaneous* changes in the average firing rate of a population of neurons (spikes s^{-1}). This population activity $A(t)$ represents the *expectation* of the fraction of N neurons to be active within a short interval Δt : $A(t) = \frac{1}{\Delta t} \frac{n(t+\Delta t)}{N}$. This quantity is commonly estimated empirically from the peristimulus time

histogram, in which the number of spikes per unit time (i.e., a rate) across a range of time bins is calculated. Peaks in the population activity reflect synchrony en masse in the neural ensemble, and thus periodic dynamics reflect phase-locked spike wave synchrony. In the neural mass formalism (in which the Wilson-Cowan equations are derived), a population is assumed to be made of a large number of identical, interconnected neurons that allows for equivalence between single neuron spiking and population spiking rates (Gerstner et al., 2014), and as such, the models are parametrised using single unit firing properties.

Using a coarse-grained, simpler model means that issues of interpretability can become more vexed. A key instance of this is the potential dissociation between neuronal firing – as measured in terms of single unit activity – and the density dynamics of populations – as measured by local field potentials and multiunit activity. In selecting a Wilson-Cowan formulation, we are committing to an interpretation of the model's latent states in terms of a beta-phase locked neuronal firing (an interpretation that is supported by experimental evidence laid out in the discussion section).

Individual Wilson-Cowan equations were used to describe each population (e.g., cortical lamina and inhibitory interneurons). Intra- and inter-laminar projections were modelled using a delayed connectivity matrix reflecting the pattern of connectivity outlined in Fig. 4A. The model is driven using $1/f^\alpha$ noise generated using a fractional Gaussian process (Dietrich and Newsam, 1993), with α a free parameter to be fit. For a full description of the model equations please see the supplementary methods IV. The model comprises three pyramidal cell layers (superficial SP, middle MP, and deep DP) plus one population of inhibitory interneurons (II). Each cell layer receives a self-inhibitory connection reflecting local synaptic gain control. The output of the model is a weighted sum (i.e., a lead field) of the layer specific firing rates with 80 % contribution from deep layers, and 10 % each from superficial and middle layers.

Priors on model parameters dictating intrinsic dynamics (e.g., time constants, firing rate properties, etc.) were chosen using a combination of sources: (1) we preferentially used the Allen Brain Atlas data portal (<https://celltypes.brain-map.org/>) and retrieved properties derived from human cortical cells; (2) when parameters were not available in Allen Brain Atlas, we used the NeuroElectro database (<https://neuroelectro.org/>) as an alternative. For both databases, multiple estimates were available per parameter, and so we used the mean and standard deviation to specify the respective expectations and precisions on (Gaussian) prior densities. The parameter priors are outlined in supplementary table I. Interlaminar connectivity was parameterised to match the same ratios of synaptic gains described in Bhatt et al. (2016). Prior covariances between parameters were assumed to be zero. See supplementary table I for specification of parameter priors.

Systems of stochastic-delay differential equations were solved numerically using a Euler-Maruyama integration scheme. For details on incorporation of finite transmission delays, and integration of the resulting system of stochastic-delay differential equations, see supplementary methods IV. To fit models, we used an implementation of the sequential Monte-Carlo Approximate Bayesian Computation algorithm (SMC-ABC; Toni et al., 2009; West et al., 2021). We take forward the maximum a posteriori (MAP) estimate (the collection of modes of the marginal posterior distributions) of each parameter for additional simulations.

Model fits were assessed with respect to the data used to fit them: *type A* – using the power spectra only; and *type B* – using both power spectra and burst features (features described in Section 2.4 “Data Features: Spectra and Distributions of Burst Amplitude/Duration”). We fit models to the group averaged data features and reduced the spectra to isolate peaks using a non-overlapping sum of Cauchy functions (see Supplementary Fig. 3 A and supplementary methods II). When fitting models across different motor states, movement preparation state was treated as a baseline, from which all other states were modulated. Movement preparation was chosen as the baseline as the group averaged

spectra from this condition exhibited the strongest beta band power. Thus, the posteriors of the movement preparation state provided empirical priors for the remaining models (i.e., Rest, Movement Execution, and Movement Imagery) that describe deviations from this baseline state. The movement preparation state was fit first using all free parameters (i.e., time constants, synaptic gains, sigmoid characteristics, properties of intrinsic and observation noise). Remaining motor states were fit using a restricted set of free parameters incorporating laminar specific time constants, synaptic gains, sigmoid characteristics, and the slope/gain of $1/f^\alpha$ innovation noise. All models were fit to the group averaged data features for each state.

2.7. Finding parameters responsible for shaping bursts

The posterior parameter estimates – under models of the motor cortex – were examined to identify parameters responsible for shaping burst properties. To do this, we individually manipulated the synaptic gain and gain parameters for the laminar specific inputs (a total of 18 parameters) on a logarithmic scale from -2.5 to $+2.5$ (equivalent to approximately decreasing or increasing the strength 12 times) in 25 steps. Each model was simulated for 48 s, and the following properties were estimated: the peak frequency of the spectrum, percentage change in power (from base model), mean burst amplitude, mean burst duration. Parameters correlating with each feature were then identified by estimating the Spearman's rank correlation coefficient with the average of each feature (i.e., the expected value of the kernel approximation to the probability density function). This constitutes a sensitivity or contribution analysis: in other words, it assesses the degree to which changing synaptic parameters generate discernible differences in the space of data features.

As features may not correlate across the whole connectivity range due to, for example, the existence of bifurcations in the model, we computed correlations within a restricted range. The optimal range was identified by computing the Spearman's coefficient between the parameter and mean feature value across all possible ranges, with a minimum window of $1/3$ of the whole range examined (i.e., 8 steps in connectivity strength). Correlations were thresholded using a Benjamini-Hochberg correction to set the False Discovery Rate to 10 %, and the range yielding the largest coefficient was selected. The correlation between average burst duration and parameter scaling was used to choose the range, as this feature was found to have the largest association with interlaminar connectivity. Correlations with the other three signal features (peak frequency, mean burst amplitude and interval) were taken within this parameter range. Finally, candidate parameters were found by examining the correlation coefficients. To identify parameters engendering changes in burst properties – but showing minimal effects on spectra – we looked for those exhibiting clear correlations with burst features but not with spectral frequency/power.

2.8. Assessment of the cortical input/output fidelity and relationship to beta bursts in spontaneous model activity

We used the constrained models to understand how parameters responsible for modifying stochastic burst activity may regulate a trade-off between beta modulation - reflecting spontaneous cortical activity - versus that induced in response to exogenous input (e.g., as arising from sensory evoked potentials). To do this we delivered a train of inputs (modulations of the asynchronous firing rate) to the middle pyramidal layer- the main recipient of thalamocortical afferents. We then assessed how this modulated beta bursts in deep cell layers – the predominant output layer of cortex (illustrated in Fig. 6). Inputs were given as a step function with random bouts of length in seconds drawn from a normal distribution with mean 500 ms and 150 ms standard deviation, and breaks drawn with mean 700 ms and 150 ms standard deviation. Inputs were multipliers on the stochastic firing rate and were set to $1\times$ on the breaks and $3\times$ (to test response to increased input rate) during bouts of

upregulation. Fidelity of modulation was assessed by computing the Pearson's correlation between the input (square wave of firing rate modulations) and output (square wave reflecting beta burst detection). We thus used this measure of input/output (I/O) fidelity to assess to what extent parameters known to regulate beta bursts also comodulate cortical integration of endo- and exo-genous activity.

3. Results

3.1. Properties of beta bursts in motor cortical activity are better than spectral features at predicting motor state

Data features summarising the spectra (e.g., peak frequency, power in band), and probability densities of beta bursts (e.g., mean burst duration/amplitude) were constructed from ECoG signals taken from the three datasets (see methods) and epoched to yield segments reflecting different motor states: rest (colour coded in blue throughout), movement preparation (red), movement execution (green), and movement imagery (orange). Data were selected from a sensor close to

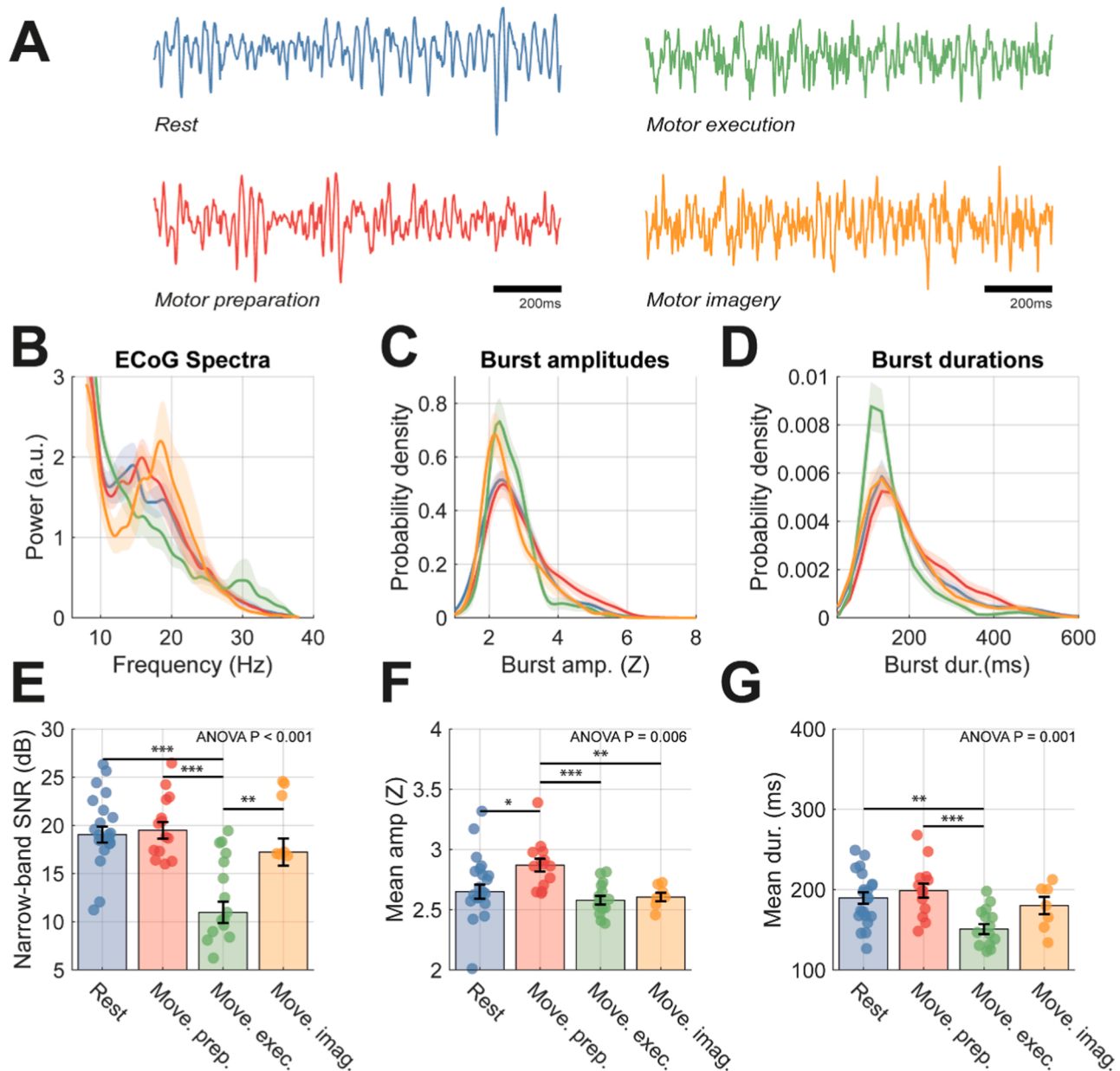


Fig. 2. Analysis of recordings from selected ECoG sensors over primary motor cortex exhibit changes in the properties of both spectral and burst features between motor states. Analyses were split between motor states: interstimulus interval (blue), movement preparation (red), movement execution (green), and motor imagery (orange). (A) Example 2 s time series of ECoG recordings for different motor states. Clear bursts of beta activity are apparent in rest, movement preparation, and imagery states. (B) Group average of the normalised power spectra, (C) probability density of burst amplitudes (Z-scores), and (D) probability density of burst durations (ms). Bar plots in (E-G) show data from individual subjects overlaid, with the group mean and standard distributions indicated by error bars. Data is shown for: (E) narrow-band SNR (dB); (F) mean burst duration (ms); (G) mean burst amplitude (Z score). Statistics indicate results of a one-way ANOVA with bars indicating respective significant post-hoc t-tests between pairs of states. An analysis of the predictive value of burst vs spectral features in classifying motor states can be found in [supplementary fig. 2](#).

primary motor cortex that exhibited the largest movement related beta desynchronisation (see methods section 1.2 for selection criteria). Example time series from the different motor states are shown in Fig. 2A which show clear bursts of 14–30 Hz beta activity in data from the different states. Spectra in Fig. 2B demonstrate movement related beta desynchronisation in the group averaged spectra that is reflected in the change in 14–30 Hz narrow-band SNR from +18 dB to +11 dB from preparation to execution of movement (Fig. 2E; post-hoc t-test (40),

$P < 0.001$). Changes were found in the wide band SNR (i.e., level of background noise indicating the overall signal quality) and corresponded to worsened recording quality during movement epochs (Supplementary Fig. 1B). Beta desynchronisation associated with movement is reflected also as a reduction in burst amplitudes (Fig. 2C and F; one-way ANOVA $P = 0.006$) and a shortening of beta burst durations (Fig. 2D and G; one-way ANOVA $P = 0.001$), although no significant changes were found in terms of the peak beta frequency or inter-burst

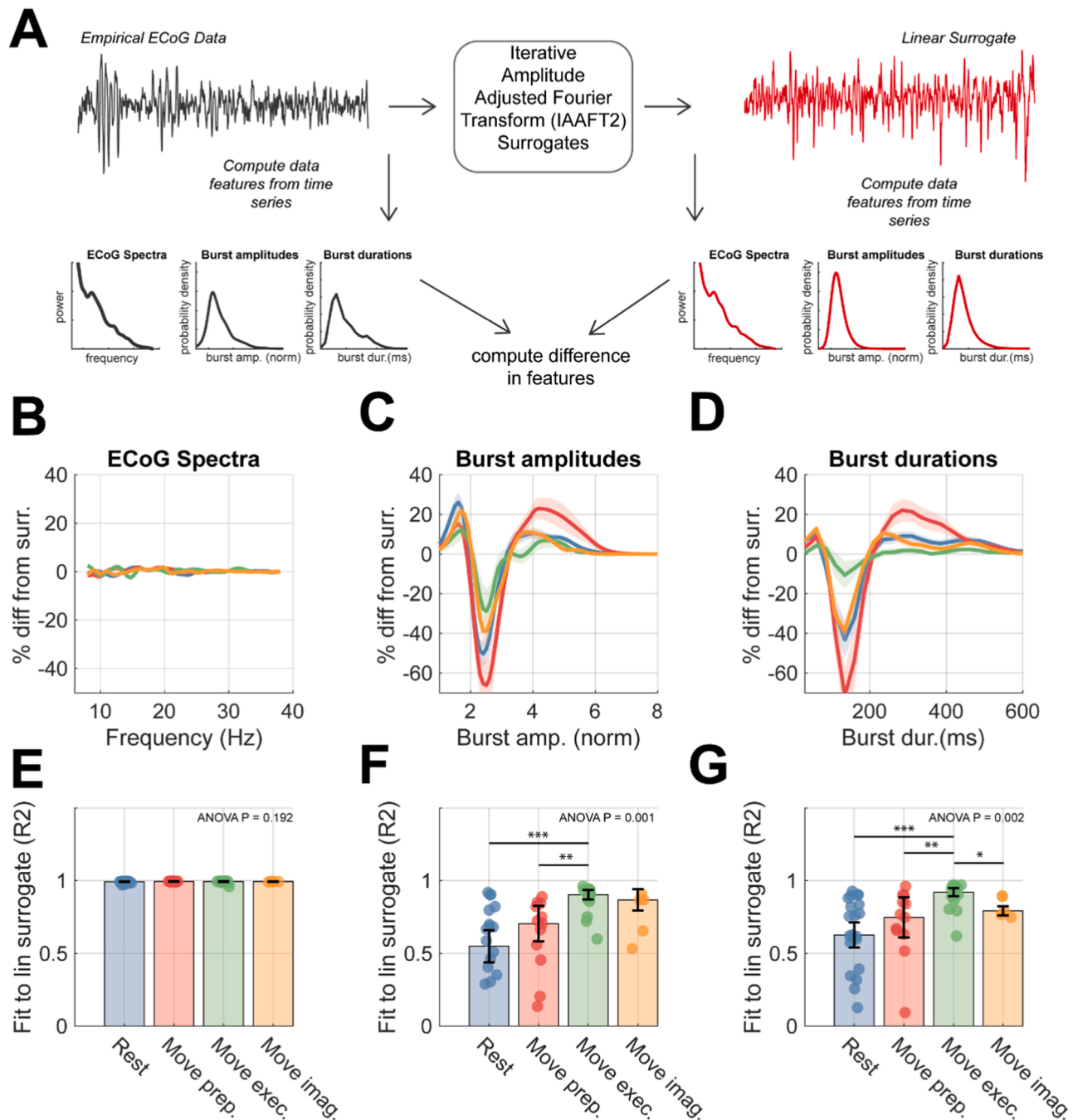


Fig. 3. Comparison of the empirical ECoG data with linear surrogates shows that burst features represent significant signal nonlinearity that is modulated across motor states. (A) An iterative amplitude adjusted Fourier transform (IAFFT; see methods) was used to construct spectrally-matched, linear surrogates (right) for each of the ECoG recordings (left). Spectral and burst features were computed for each signal, and the difference between the surrogate and empirical features were compared to assess the extent to which nonlinearities were present in the data from the four motor states. (B) Plots showing the averaged difference between surrogate and empirical power spectra (computed as a percentage change). (C) Same as (B) but for distributions of burst amplitudes. (D) Same as (B) but for distributions of burst duration. (E) Bar chart indicating the median goodness-of-fit of the surrogate to empirical data feature with interquartile range indicated by error bars. (F) Same as (E) but for burst amplitude distributions. (G) Same as (E) but for burst duration distributions. Statistics indicate results of one-way ANOVA with bars indicating respective significant post-hoc t-tests between pairs of states.

intervals (Supplementary Fig. 1 C and D, respectively). These results are robust to the choice of threshold used to define bursts, with peak discrimination between motor states occurring in the region of the 70th to 85th percentile (Supplementary Fig. 5 A and B). An analysis of the spatial distribution of ECoG activity over the cortex (Supplementary Fig. 7) in a representative subject, showed that beta power, burst amplitude and durations peaked at a location close to the motor cortex.

To compare the predictive value of either spectral or burst features, we trained an ensemble of binary SVM classifiers to predict different motor states (Supplementary Fig. 2). Decision boundaries (indicating > 50 % or > 75 % prediction success) between all four motor states were present for classification with burst features, and AUCs of the receiver operating characteristics (ROCs) showed good predictive value (AUC > 0.80). In contrast, classifiers using summary statistics derived from the power spectra could only separate features from movement preparation and execution states with AUCs > 0.5 (greater than chance level) and could not classify features derived from rest or imagery states. These results suggest that, when using band restricted information (i.e., within 14–30 Hz), the properties of bursting activity can significantly augment the prediction of motor states from brain activity.

3.2. Burst features are not predicted by linear models of the data

To further determine whether beta burst features reflect meaningful information about the underlying motor state, beyond that contained in

the spectra, we compared empirical features with those computed from spectrally matched IAAFT surrogates (see methods Section 3.4). In Fig. 3, we show a comparison between empirical data features and the average feature derived from surrogate data ($n = 25$) for each of the motor states. By design, the surrogates matched well to the power spectra of the data (Fig. 3B and E). Differences between the distributions of burst amplitudes and durations computed from the data or from linear surrogates (Fig. 3C/F and D/G, respectively) show that both features deviate significantly (median $R^2 < 0.80$) from that expected under linear assumptions. Comparisons of the goodness of fits (R^2) to linear surrogates showed that deviations in burst amplitude distributions from linearity were not identical across motor states (Fig. 3F, one-way ANOVA $P = 0.002$), with movement preparation and rest states showing reduced R^2 values when compared to movement execution. Similarly, burst durations exhibited significant changes between states (Fig. 3G, one-way ANOVA $P = 0.002$) with data from the rest and movement preparation providing the greatest evidence for nonlinearity among all the motor states. These data suggest that burst features represent underlying nonlinearities in the data that are not captured in the power spectra alone. States associated with rest and movement preparation are associated with a higher degree of nonlinearity, especially when compared to movement execution. We next use a neural mass model to investigate the potential biophysical explanations for these differences.

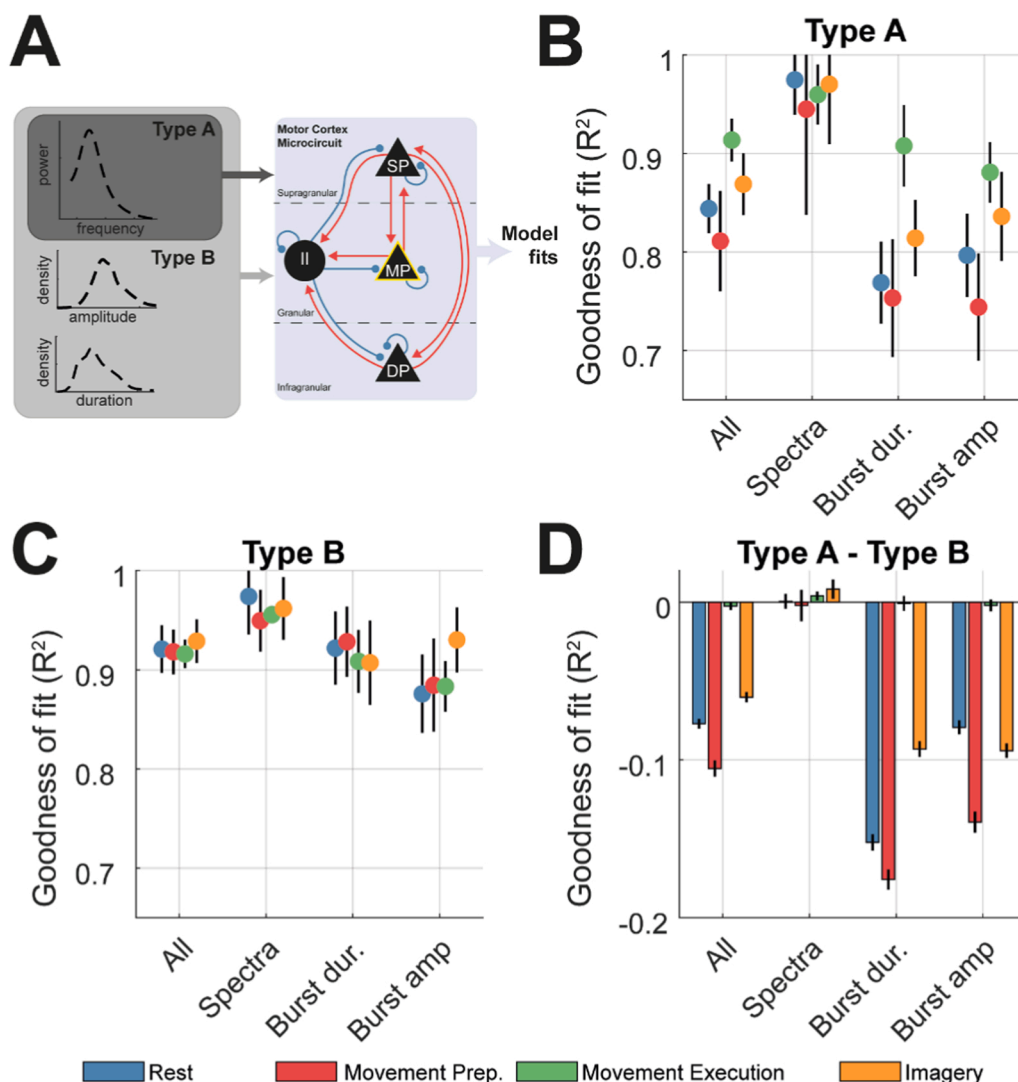


Fig. 4. Comparison between type A (spectra only) and type B (spectra + burst features) fits of the motor cortex microcircuit model demonstrates that spectral features are not sufficient to accurately predict burst features. Predicted data features were constructed by simulating data using draws from the posterior distributions over parameters ($n = 256$). (A) Schematic of the motor cortex microcircuit model. Each black node represents a neural mass that is coupled with either excitatory (red) or inhibitory connections (blue). There are three pyramidal cell layers: superficial (SP), middle (MP), and deep (DP), plus an inhibitory interneuron (II) population. Model parameters were constrained using either pre-processed spectra (type A) or both the spectra and burst features (type B). (B) Summary of the median \pm SEM goodness of fit (R^2) of the model to data from each state resulting from type A model fits. (C) Same as (A) but for type B model fits. (D) Difference in the goodness-of-fit (ΔR^2) between type A and B fits. Negative values indicate accuracy was greater in type B than type A fits.

3.3. Biophysical models of motor cortex constrained to fit power spectra do not predict distributions of burst features

The SMC-ABC algorithm was used to constrain a biophysical (neural mass) model of the primary motor cortex microcircuit to key data features (i.e., the power spectral densities and probability densities of burst duration/amplitude) from each of the four motor states. Models were fit to the group averaged data features and reduced spectra (see [Supplementary Fig. 3D-F](#) and supplementary methods II). To assess the value of the power spectra in predicting burst features, fitting procedures were split into two groups depending upon the data features used: *type A* - constrained exclusively using the spectra, or *type B* - constrained using a combination of the spectra and distributions of burst amplitude and duration ([Fig. 4A](#)). Samples of the simulated time series using posterior estimates, as well as the fitted features are shown in [Supplementary Fig. 3](#).

Type A models fit well to spectra ([Fig. 4B](#); all states $R^2 > 0.90$) but showed that spectra were not sufficient to predict burst features accurately. Further analysis of the fitted features ([Supplementary Fig. 3E and F](#)) showed that predicted distributions of burst amplitudes were attributable to smaller amplitude bursts than those observed in the experimental data, and burst durations were shorter than predicted in the case of rest and movement preparation (blue and red, respectively; $R^2 < 0.80$). However, *type A* fits were sufficient to accurately recover the empirical distributions of burst durations during movement execution ([Fig. 4C](#); green, $R^2 > 0.90$).

In contrast, *type B* fits demonstrate that the model parameters could reproduce burst features ([Fig. 4C](#)), with a median fit of $\sim 92\%$ for all features. Complementary to the analyses of feature nonlinearity in [Fig. 3](#), we show that models of rest and movement preparation (the motor states exhibiting the highest degree of nonlinearity) gained the most (in terms of accurate predictions) from the explicit inclusion of burst features (difference of *type A* and *B* fits shown in [Fig. 4D](#)). In contrast, for data from movement imagery and execution, there was less gain in accuracy when explicitly incorporating burst features. In [Supplementary Fig. 5](#), we analysed the dependency of model inference upon the specific threshold used to defined bursts. This analysis shows that both parameters and models were not as well constrained at higher thresholds, due to the increase in variance in the summary statistics that arises from the drop in the number of instances identified.

The inadequacy of *type A* fits in predicting burst features (i.e., features withheld from *type A* model inversions) suggests that burst characteristics are the product of circuit mechanisms (and associated biophysical parameters) that are either independent or at most only weakly associated with those governing the power spectral amplitude and implies that features summarising temporal organisation of bursts are important for informing neural models. Furthermore, burst features from periods of rest and preparation appear most different from those predicted using *type A* fits. In the next section we aim to identify parameters of the fitted microcircuit models of motor cortex underlying these changes in burst properties.

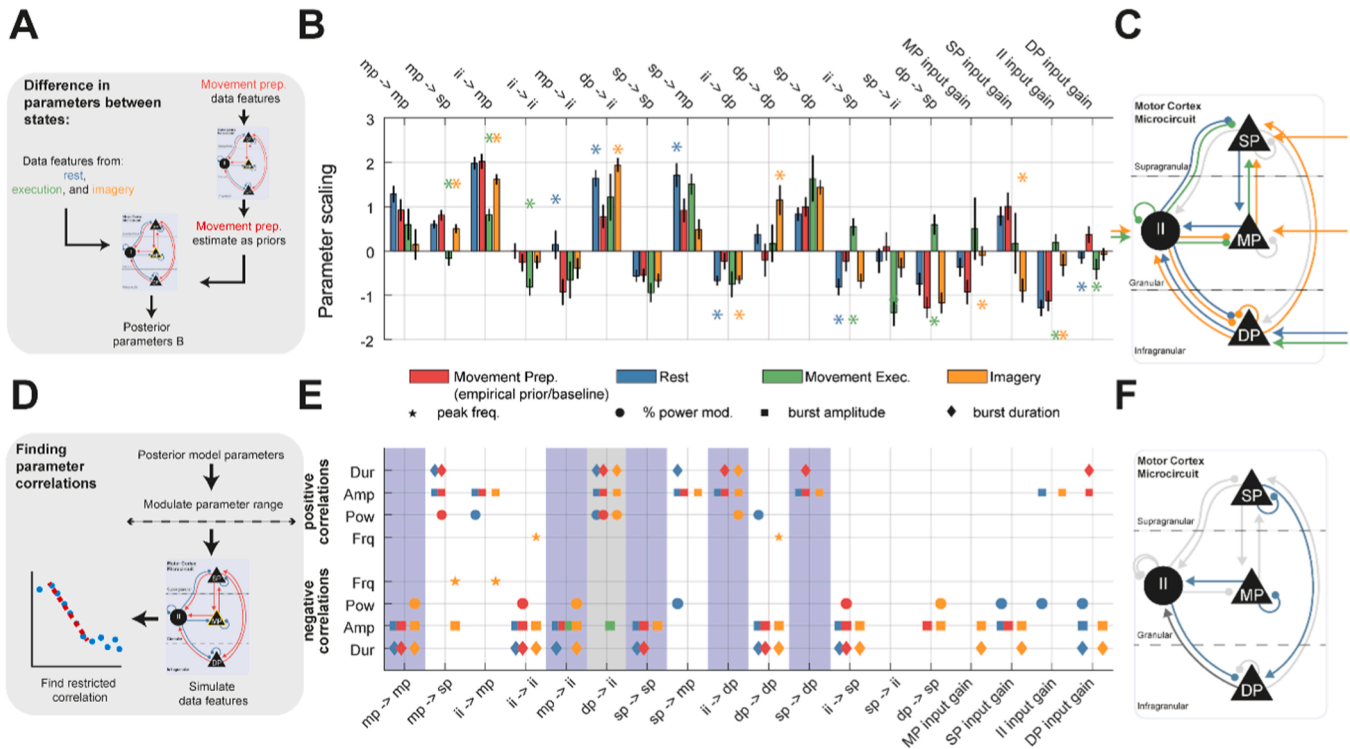


Fig. 5. Results of the motor cortex model fits to ECoG data from different motor states. This analysis shows posterior model estimates, as well as the modulations of parameters from the baseline condition (movement preparation), as well as a correlation analysis of circuit parameters with the statistics of spectral and burst features resulting from posterior simulations. (A) Parameters of the model of motor cortex microcircuit were estimated from fits to group averaged data features from all four motor states using ABC-SMC. (B) Bar plot of the posterior model parameters with y-axis indicating log scaling \pm the prior values at 0. Asterisks indicate statistically significant changes (Z-test of posteriors, $P < 0.05$) in parameters from the baseline state (movement preparation state; red). (C) Connections exhibiting a significant modulation are shown on the colour coded circuit diagram. (D) Modulations in parameters were estimated by first fitting to movement preparation data as a baseline state (using a wider set of free parameters, see methods), and then using these as empirical priors on the remaining models (using a smaller set of free parameters, see methods). (E) Parameters of the posterior models dictating interlaminar connectivity, and laminar specific inputs were then systematically examined for correlation with different data features. Correlations were performed on a restricted range with minimum range equal to $1/3$ of the total parameter space tested (see methods). Parameter significance was determined using a False Discovery Rate correction (set to 10%). Grey bands highlight parameters that modulated both power and burst features. Parameters in light grey reflect those predominantly acting on burst features. (F) Connections and inputs exhibiting a significant correlation with either spectral and burst features (highlighted in grey) or exclusively burst features (blue) are shown on the colour coded circuit.

3.4. Modulation of interneuron activity in the microcircuit is predominantly responsible for modulation of beta bursts

Parameters of the fitted models exhibited significant deviation from the empirical priors provided by model fit to movement preparation (i. e., the baseline state), and indicate changes in intra- and inter-laminar coupling (Fig. 5A and B). As expected, movement execution and imagery displayed the largest changes in parameters away from the movement preparation state. Movement execution largely involved changes in interneuron inhibition of middle and superficial layers (MP and SP, respectively; green Fig. 5C). Movement imagery and rest were associated with strengthening of reciprocal loops between deep and interneuron (DP and II, respectively) cell layers (orange and blue, Fig. 5C). An analysis of the laminar specific activity in the model (Supplementary Fig. 8) demonstrated that these two layers (DP and II) were most active during burst activity in the movement preparation state, with firing rates in inhibitory layers greatest at the peak of a burst. We note that the baseline inhibitory tone (dashed line in supplementary figure) is high (~50 Hz) when compared to the activities of the pyramidal layers (~10 Hz). Both deep and inhibitory layers were heavily recruited during bursts and exhibit sustained rhythms outside of the main burst but with irregular phases that averages out across different instances.

To identify the parameters responsible for shaping beta burst features, we systematically altered interlaminar connection strengths and input gains, and then applied a restricted-window correlation analysis (see methods section 1.7) to detect co-modulation of certain parameters with the predicted spectral frequency, beta power, mean burst duration, or mean burst amplitude (Fig. 5D). Panels 5E and F show that several parameters affect these data features. For instance, the strength of DP→II connectivity (highlighted in grey in Fig. 5E) positively correlates with both burst duration/amplitude and spectral power for 3 out of 4 of the states. Five parameters were found to predominantly modulate burst amplitude and durations independently of power (light blue in Fig. 5D, not showing correlation with spectral frequency or power for rest or movement prep.): MP → MP, MP → II, SP → SP, SP → DP, and II → DP. Notably, 4 out of 5 of these parameters involved modulation of inhibitory interneurons. To investigate how these parameters shape beta dynamics, we chose an example parameter – SP self-inhibition – that we took forward for further analysis. This was because: (A) it assumes a similar strength between motor states (Fig. 5B); and (B) it negatively correlates with both burst amplitude and duration but exhibits only limited effects on spectral peak frequency or power (Fig. 5E). It should be noted that this analysis depends on the minimum range for correlation detection, as well as the significance threshold. However,

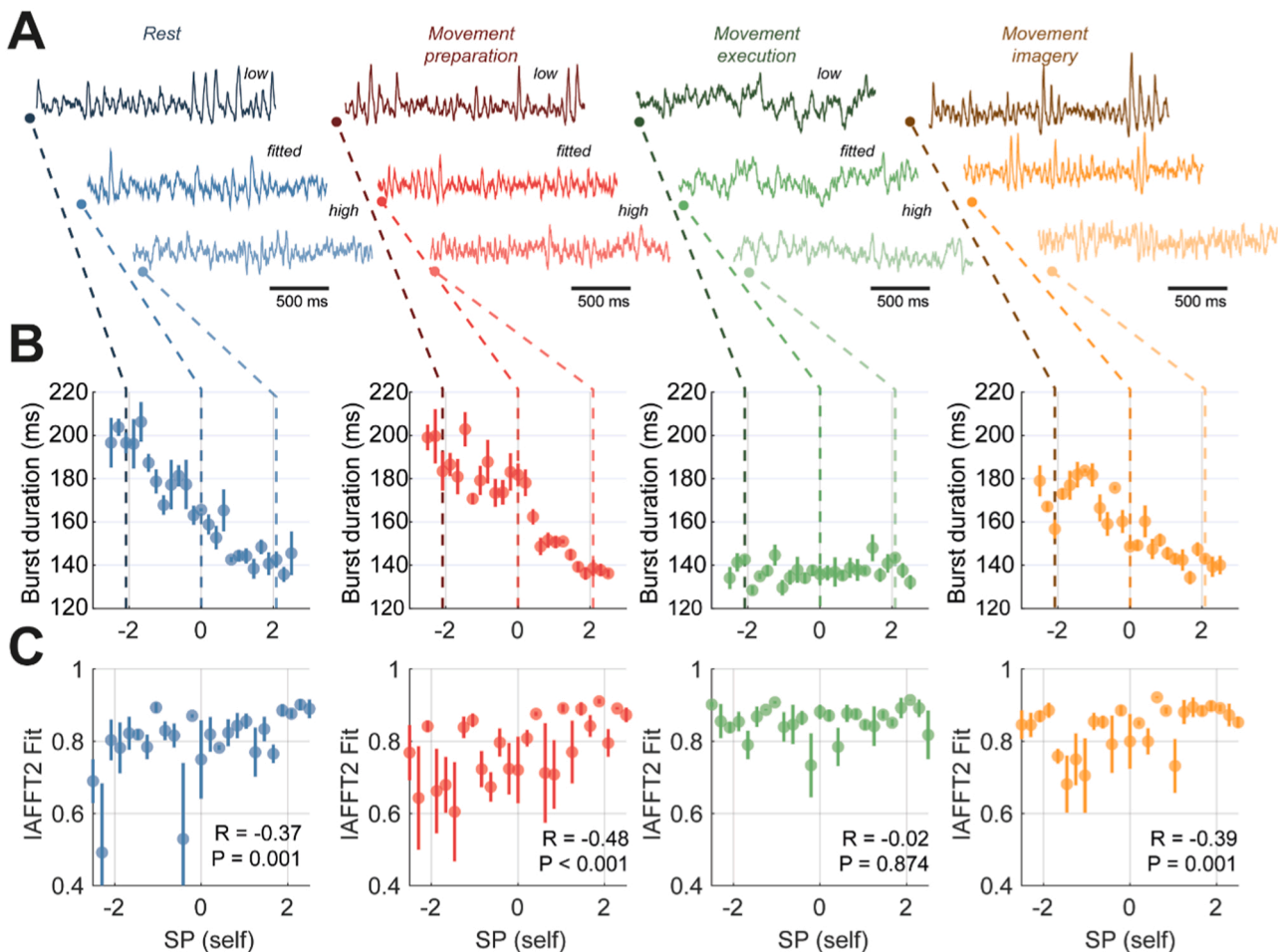


Fig. 6. Detailed analysis of the modulation of simulated population activity in the primary motor cortex associated with changes in the strength of superficial pyramidal layer (SP) self-inhibition and corresponding correlations with burst duration and nonlinearity. The level of superficial layer self-inhibition was used as a control parameter following from the correlation analysis presented in Fig. 5. Simulations were performed on a range of parameter values spanning -3 to $+3$ (log scaling on the posterior). (A) 1.5 s of sample data simulated from each model of a motor state at either low (-2 scaling), fitted (0 scaling), or high ($+2$ scaling). (B) The mean burst duration is plotted against the strength of SP self-inhibition. All states excluding movement execution indicate existence of negative correlation between control parameter and burst duration. (C) The goodness of fit between burst duration distributions estimated from simulated data and linear surrogates (IAAFT processes) indicates that the degree of nonlinearity in the signals is anticorrelated to changes in the burst durations. Inset stats give the correlation coefficient and P-value for test of association between burst duration and the IAAFT R^2 value.

correlations with burst duration and amplitude were preserved despite these choices.

3.5. Increased interneuron inhibition of superficial layer acts to shorten cortical beta bursts

We used SP self-inhibitory gain as a control parameter to investigate the effects of altered laminar specific inhibition on the temporal organisation of simulated neural activity (Fig. 6A). Sustained oscillatory activity is observed in models fit to the data recorded during rest, movement preparation and movement imagery states, with strengthening of inputs of the superficial layer interneurons acting to extend bursts. Corresponding intermittencies in beta rhythms were graded, with burst durations shortening as SP self-inhibition was increased (Fig. 6C; blue, red, and yellow). In the model fit to data recorded during movement execution (in green), there was no periodic behaviour in the simulated traces generated by the model (Fig. 6A and B, green).

We also analysed changes in feature nonlinearity (using comparison to IAAFT surrogate method introduced in Section 3.2; Fig. 6C), in which we found that IAAFT fits were negatively correlated with burst duration for three of the four states. However, the IAAFT R^2 exhibited a higher degree of variance than burst durations, suggesting that the latter might be a better proxy for system state in real-world data. These analyses demonstrate that the duration of temporal intermittencies of beta rhythms in the model, can be explained by the impact of biophysical parameters on the system, in this instance, SP self-inhibition acts to dampen rhythmic beta responses in motor cortex outputs.

3.6. The temporal organisation of spontaneous beta bursts correlates with cortical integration of exogenous inputs

Lastly, we investigated the hypothesis that cortical beta burst properties reflect a trade-off between integration of spontaneous endogenous activity, versus that arising due to structured exogenous inputs (Karvat et al., 2021) (i.e., from sensory or higher order thalamus). In Fig. 7A and B we illustrate an in-silico experiment conducted on the models fit to different motor states in which we delivered patterned modulations of asynchronous (i.e., noisy) inputs to the middle layer of cortex (the main recipient of thalamic projections). We considered beta bursts in the deep layer (the main projection layer of cortex) as the cortical output. We then measured the correlation between the input and output as an estimate of transmission fidelity.

The results in Fig. 7C show that whilst strengthening either SP or MP layer specific interneuron inhibition decreased the mean burst duration (right axes; shown by circle markers), the correlation with I/O fidelity was reversed dependent upon the parameter that was chosen for modulation. For instance, in the models fit to rest data, SP self-inhibition induced a shortening of bursts that correlated with a decrease in I/O fidelity. The opposite was true for modulations of MP self-inhibition. The analysis in Fig. 7D, shows that for all of the five parameters identified to modulate bursts (i.e., shaded blue in Fig. 5E), three parameters displayed positive correlations between I/O fidelity and burst duration.

An analysis of the excitation/inhibition (EI) ratio was performed by taking the ratio between the mean excitatory and inhibitory inputs to the DP cell layer (summarised in supplementary Fig. 6). We then investigated how EI changed between bursts. The results (Supplementary Fig. 6) show that when modulating the strength of either SP or MP self-inhibition, both connections (as expected) tipped EI balance in favour of inhibition during beta bursts. We found that there was no consistent correlation with IO transmission fidelity, with positive or negative correlations found for modulations of either MP or SP inhibition, respectively.

These findings suggests that the properties of spontaneous cortical activity can reflect the underlying balance of cortical integration of endogenous and exogenous inputs. This comes with the caveat, that to infer cortical processing from the temporal organisation of spontaneous

activity requires a priori knowledge of the laminar interactions that are responsible.

4. Discussion

4.1. Summary of findings

Temporal dynamics of spontaneous activity in the brain contain significant information regarding how the cortex processes incoming information. Here, we have shown that motor states can be decoded from electrocorticography using features computed from narrow-band beta activity (Fig. 2). Our results show that these features aid brain state classification (Supplementary Fig. 2) and arise from signal nonlinearities that are not detectable in the power spectrum (Fig. 3). Further, evidence for nonlinearity was found to be greatest in data recorded during rest and movement preparation, indicating that the increase in information, beyond that available in the spectrum, and contained in the distributions of burst amplitude/duration, is greatest in these states. Using a neural mass model, we then delved into the potential mechanisms and their functional significance. As expected, we found that neural mass models fit exclusively to spectra were not sufficient to accurately recapitulate the features of cortical beta bursts (Fig. 4). Analysis of the fitted model parameters between motor states found that burst properties are modulated predominantly by connections altering interneuron inhibition and arise independently of connections modulating spectral amplitude or frequency (Fig. 5). Using the strength of superficial self-inhibition as an exemplar control parameter, we showed that layer specific inhibition acts to stabilise beta bursts in the time domain (Fig. 6). Finally, using the microcircuit model, we showed that the same parameters found to modulate temporal organisation of spontaneous activity, also control the balance by which the cortex integrates exogenous inputs with that of ongoing endogenous activity (Fig. 7).

4.2. Intermittencies in bursts can discriminate brain states associated with movement

Transient fluctuations in neural oscillations can contribute to the understanding of the organisation of brain activity (Bonaiuto et al., 2021; van Ede et al., 2018; Feingold et al., 2015; Lundqvist et al., 2016; Sherman et al., 2016; Shin et al., 2017). Transients in beta oscillations, the focus of this study, are found in healthy sensorimotor cortex (Feingold et al., 2015; Hannah et al., 2020; Little et al., 2019; Rule et al., 2017; Wessel, 2020), and also play a prominent role in Parkinsonian electrophysiology (Cagnan et al., 2019; Tinkhauser et al., 2017b). Quantification of these intermittencies is beginning to build up a taxonomy of bursts by identifying changes associated with different brain states and diseases (Deffains et al., 2018; Enz et al., 2021; Khawaldeh et al., 2020; Shin et al., 2017; Torrecillos et al., 2018). The discrimination of brain states by temporal features, as well as their transitory nature, makes them attractive targets for closed-loop approaches to neuromodulation, for instance using either beta (Little et al., 2016; Tinkhauser et al., 2017a; West et al., 2022), or theta and gamma (Kanta et al., 2019; Knudsen and Wallis, 2020) frequency based biomarkers.

The results reported here support this approach by providing direct evidence that quantification of burst duration and amplitude, from narrow-band signals can aid classification of motor states, in a way that is superior to that achieved when using spectral measures of beta power or peak frequency alone. Notably, we were able to discriminate between periods of rest and movement preparation, despite a similar beta SNR observed across these states. These burst features are good candidates for control signals in closed loop neuromodulation, as they can be readily computed from narrowband data such as that available on current sensing/stimulation devices such as Percept (Medtronic) (Van Rheede et al., 2022) and they are known to be modulated by deep brain stimulation (Pauls et al., 2022). Additionally, motor state discrimination

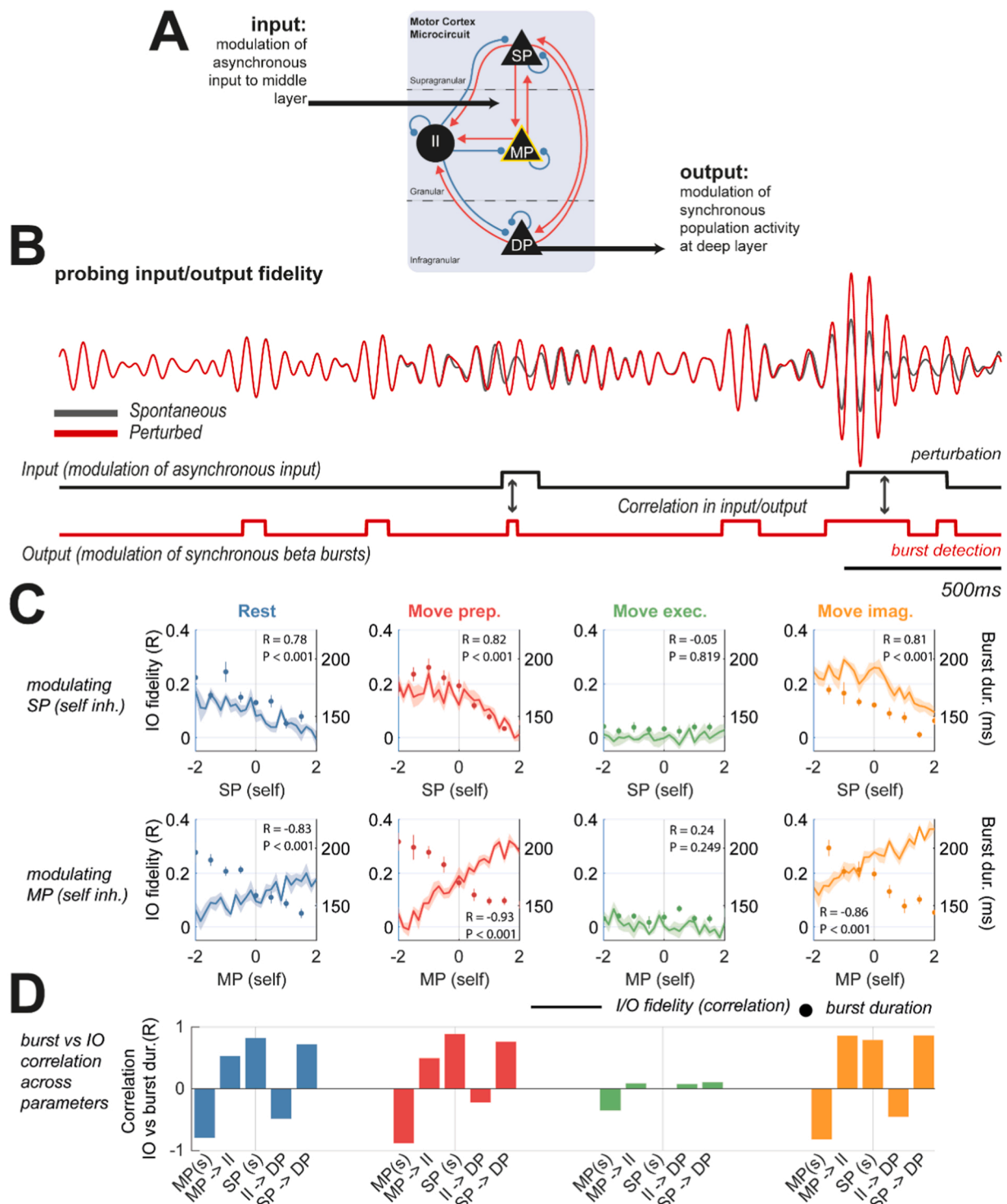


Fig. 7. Parameters responsible for modulating burst properties do not uniformly alter the fidelity of synchronous cortical responses to exogenous inputs. (A) To probe the fidelity of cortical beta responses to changes in exogenous input, fitted models were used in an in-silico experiment. Asynchronous (stochastic) inputs to the middle layer were modulated with a square wave of random intervals. Beta burst detections in simulated signals from the deep cell layers were taken as the outputs. The total “fidelity” of input/output (I/O) transmission was estimated using the Pearson correlation between these two square waves. (B) Example waveforms of the spontaneous (unperturbed; grey) activity, overlaid with perturbed (in red) activity matching the perturbation (i.e., modulation in noise to middle layer) seen below (black square wave). The output of the system matches the beta burst detections (red square wave) (C) Plots of I/O fidelity (left axis) and burst duration (right axis) when modulating either SP or MP self-inhibition (top and bottom rows, respectively). Inset statistics indicate Pearson’s correlation R between I/O fidelity and burst duration and corresponding P value. (D) Bar plot indicating correlation between I/O fidelity and burst duration for five parameters known to modulate burst properties (see Fig. 5). Note the direction of correlation changes depending upon which parameter is being modulated.

was enhanced compared to linear surrogates, with the degree of nonlinearity being largest during rest and movement preparation (Fig. 3). This technique has previously been deployed to show that Parkinsonian beta bursts are more nonlinear when compared to a medicated control state (Duchet et al., 2021). This suggests the possibility that biomarkers relating to signal nonlinearity can also form the basis for novel closed loop control algorithms (Jelfs et al., 2010).

4.3. Mechanisms and functional implications of bursts in the motor cortex

If the statistics of bursts in rhythmic neural activity are discriminating features of brain states, then they may provide a window into the underlying changes in the generative neural circuitry. A prominent model of beta bursts, consisting of high amplitude, short duration events over the sensorimotor cortex, highlights the importance of synchronous subthreshold inputs to proximal and distal dendrites of pyramidal neurons (Bonaiuto et al., 2021; Sherman et al., 2016). Strong inputs to distal dendrites may then halt information processing by recruitment of inhibitory interneurons in the supragranular layers (Jones et al., 2009), that can lead to a reduction in pyramidal firing rates following cortical beta bursts (Karvat et al., 2021). As with any model, the conclusions drawn are a product of the data feature that they wish to explain. In the case of Sherman et al. (2016), bursts were comparatively rare (98th percentile amplitude threshold; ~ 0.5 burst s^{-1}), high amplitude events that permitted well stereotyped waveforms. In our own analysis, we aimed to explain more common events (75th percentile amplitude threshold; ~ 1 – 1.5 burst s^{-1}) that were typically multicycle. Similar events have been shown to exhibit burst distributions extending up to ~ 300 ms in duration (Seedat et al., 2020). A focus on high amplitude beta events may occlude alternative mechanisms by which recurrent interlaminar interactions may either generate and/or sustain beta bursts lasting multiple cycles.

As changes in the temporal structure of beta rhythms between motor states are ascribable to alterations in inter and intra laminar connectivity, it follows that the amplitude modulation of beta oscillations may reflect changes in the cortical response to exogenous inputs. The cortex is known to exhibit context dependent changes in interlaminar propagation and laminar specific inputs (Kirchgessner et al., 2020; Takeuchi et al., 2011) yet limited information is known regarding the changes occurring during movement (Inagaki et al., 2022), and even less about how this relates to rhythmic neural activity. Our simulations demonstrate that input/output relationships between exogenous modulations in asynchronous firing rates and entrainment of cortical outputs at beta frequencies may change between brain states. Previous work has suggested that balanced excitation and inhibition can facilitate gating of neural signal propagation (Vogels and Abbott, 2009), we however did not observe a consistent relationship between EI balance and cortical beta responses to sensory inputs (Supplementary Fig. 6), perhaps due to the high resting inhibitory tone in the model.

Further we show that properties of spontaneous activity such as burst duration can correlate with the fidelity of cortical integration of exogenous inputs (Fig. 7). However, the direction of this relationship is mechanism dependent – and thus inference of properties of cortical processing from analysis of spontaneous burst activity, would require a prior knowledge on the connections responsible for their modulation. Thus this work provides support for the idea that, given suitable generating circuitry, bursts in sensorimotor cortex can reflect a competition between spontaneous and sensory evoked activity (Karvat et al., 2021). It is possible that this cortical gating of sensory information may occur in tandem with transient changes to subcortical circuitry during sensorimotor processing (Mirzaei et al., 2017).

4.4. Model inference and intermittent dynamics

This work also provides evidence that power spectra alone may contain insufficient information to accurately constrain parameters of

nonlinear and/or stochastic models. Existing dynamic causal models of large scale temporal dynamics such as Parkinsonian beta bursts (Reis et al., 2019) or epileptic seizures (Rosch et al., 2018) appeal to fast-slow separation of time scales (i.e., the adiabatic approximation) in which changes in dynamics (i.e., bursting to quiescence) can be approximated by a model of fast (i.e., oscillatory) dynamics, with slow variables regulating the transition between states (Jafarian et al., 2021). In a similar vein, many phenomenological or statistical models describe bursts as a transition between discrete dynamical states (Heideman et al., 2020; Seedat et al., 2020). Other modelling approaches, such as that of Sherman et al. (2016), described above, take well constrained compartmental models that can describe high amplitude beta events, albeit with a specific pattern of input and in the absence of endogenous activity.

In this paper we take a different approach and treat bursts as the product of stochastic “quasi-cycles” that arise from noise driving a stable system such as a damped oscillator (Powanwe and Longtin, 2019), that exhibit amplitude envelopes that can be modelled in terms of a drift-diffusion process (Duchet et al., 2021). Thus we use a model incorporating the full nonlinear transfer functions, and fit parameters of the resultant stochastic differential equations (West et al., 2021). Given the full breadth of information summarised by both the spectra and distributions of burst features, these models can well describe temporal dynamics of ECoG data in a parsimonious way without needing to appeal to modelling multiple states separately.

The distinction between generative models in which synaptic parameters fluctuate slowly and our model based upon stochastic dynamics speaks to an important distinction between explanations for itinerant dynamics of which beta bursts provide a good example. Technically, the first kind of generative model rests upon *structural instability*, where the itinerant changes in fast neuronal dynamics – and ensuing transients – are generated by changes in the fixed points of a system with the parameters of the equations of motion. In contrast, the second kind of generative model relies upon *dynamical instability*; namely, unstable (or weakly stable) fixed points to produce transient dynamics. This formal distinction has importance for understanding the biophysical mechanisms that generate bursts in population activity, as well informing stimulation approaches that aim to modulate them. For instance, in the case that bursts are the direct product of slow changes in neural circuits (i.e., invoking neural plasticity), then stimulation should directly target these mechanisms, whereas in terms of dynamical instability, stimulation can be patterned to with the aim of suppressing transient burst activity, or disrupting neural states that preclude them.

4.5. Limitations

A major problem when investigating changes in temporal dynamics between brain states arises from potential confounds that arise from the effects of changes in overall signal-to-noise of recordings. Although we found changes in the wide-band SNR (i.e., an estimate of signal quality between states (Supplementary Fig. 1), alterations in burst amplitude did not correlate with either wide- or narrow-band SNR. Further, bursts were defined using a window-specific threshold, which prevents burst properties from predominantly reflecting SNR differences – a problem encountered when using a common (i.e., across condition) threshold (Schmidt et al., 2020). The robustness of using a fixed threshold of 75th percentile is well supported following reports that specific threshold values do not qualitatively change outcomes of burst analyses (Lofredi et al., 2019; Tinkhauser et al., 2017b). Our analyses here support this and show that separability of motor states is maximal around the 70th to 85th percentile. Further, higher thresholds require more data to stabilise estimators of burst duration or amplitude. Accordingly, we found that at these higher thresholds, the precision of parameter inference from models was decreased.

We applied selection criteria (described in methods Section 2.2) that lead to the rejection of ~ 40 % of the available data, as in these subjects

there was no beta peak at rest or movement preparation that was responsive to movement. Such stringent criteria were chosen to ensure that mechanistic modelling of the data was focused upon clear-cut cases in which intermittencies in beta were unobstructed by limits in signal quality. It is likely that in many cases of data rejection, the sparse spatial sampling of the ECoG grid may impede the recording from the underlying cortical source.

Additionally, model inversion with Approximate Bayesian Computation is susceptible to issues arising due to insufficiency of the summary statistics (i.e., the power spectrum, or distributions of burst duration/amplitude used here). More complete descriptions may be achievable with the bispectra (i.e., the Fourier transform of the third-order cumulant; Halliday et al., 1995). The results of the current study clearly call for development of generative models of these kinds of data features.

The ECoG signal arises primarily from an aggregate of currents flowing along the dendrites of spatially aligned pyramidal cells, a state not directly modelled by the Wilson-Cowan equations, which instead describe firing rates. Thus, the adoption of this model comes with an implicit appeal to an interpretation of the model's states in terms of beta frequency phase locked neural firing. The frequency specific power of signals such as that measured in the local field potentials/ECoG and single unit firing rates can be dissociated (Confais et al., 2020; Rule et al., 2017). However, recent work by Karvat et al. (2021) has demonstrated that the instantaneous population firing rate (as commonly estimated in a peri-stimulus spike histogram, and the state described by the Wilson-Cowan model), exhibits correlation with high amplitude beta frequency bursts in the LFP. Previous work analysing spike/field synchrony has reported correlations spanning from weak (Rule et al., 2017), up to highly significant (Murthy and Fetz, 1996a, b; Peles et al., 2020).

The coarse graining of the neural mass model lumps diverse populations of interneurons into a single homogenous description. This limits the extent to which the model can explain important contributions from the neurochemical diversity of cortical interneurons (i.e., parvalbumin and somatostatin neurons). This diversity is known to play important roles in the modulation of large-scale rhythmic activity at both the gamma and beta frequencies (Chen et al., 2017; Lee et al., 2013; Veit et al., 2017). Future models can finesse the exploration of the role of interneuron diversity by inclusion of separate neural populations furnishing their specific electrophysiological properties and anatomical distributions.

4.6. Conclusions

This work provides significant evidence that the temporal properties of bursting intermittencies in brain rhythms contain unique information about the underlying circuits that generate them, beyond that more conventionally inferred from the power spectra of electrophysiological data. Furthermore, we have shown that burst features are nonlinear and are not simple predictions of the power spectra. Using a model of the primary motor cortex's microcircuitry, we show that bursts can arise from stochastic dynamics, with properties that are predominantly modulated by laminar specific inhibitory loops. We have shown that this has important consequences for understanding information processing in cortical microcircuits, with simulations demonstrating a non-trivial relationship between burst duration and the responsiveness of the cortex to exogenous inputs. These findings inform novel paradigms to understand the role of external perturbations such as electrical brain stimulation, in manipulating cortical computations when in the presence of spontaneous fluctuations in neural rhythms.

Data availability

The data used in this work were taken from a publicly accessible library published by Kai Miller and can be found at <https://purl.stanford.edu/zk881ps0522>. The code used to produce the analyses, as well as model simulations presented in this paper can be found in the

following Zenodo archive: <https://doi.org/10.5281/zenodo.7509926>.

Acknowledgements

H.C. is supported by Medical Research Council UK Award MR/R020418/1. K.J.F. is supported by funding for the Wellcome Centre for Human Neuroimaging from the Wellcome Trust (205103/Z/16/Z), a Canada-UK Artificial Intelligence Initiative (ES/T01279X/1) and the European Union's Horizon 2020 Framework Programme for Research and Innovation under the Specific Grant Agreement No. 945539 (Human Brain Project SGA3). S.F.F. acknowledges personal funding support from the UCLH Biomedical Research Centre. B.D. is supported by Medical Research Council grant MC_UU_00003/1. We thank Ashwini Oswal for code sharing and insightful discussions of this work. We also thank all authors of the publicly available toolboxes used in this paper (listed in the supplementary information).

Appendix A. Supporting information

Supplementary data associated with this article can be found in the online version at doi:10.1016/j.pneurobio.2022.102397.

References

- Adamantidis, A.R., Gutierrez Herrera, C., Gent, T.C., 2019. Oscillating circuitries in the sleeping brain. *Nat. Rev. Neurosci.* 746–762.
- Baker, A.P., Brookes, M.J., Rezek, I.A., Smith, S.M., Behrens, T., Probert Smith, P.J., Woolrich, M., 2014. Fast transient networks in spontaneous human brain activity. *eLife* 3.
- Bhatt, M.B., Bowen, S., Rossiter, H.E., Dupont-Hadwen, J., Moran, R.J., Friston, K.J., Ward, N.S., 2016. Computational modelling of movement-related beta-oscillatory dynamics in human motor cortex. *Neuroimage* 133, 224–232.
- Bonaiuto, J.J., Little, S., Neymotin, S.A., Jones, S.R., Barnes, G.R., Bestmann, S., 2021. Laminar dynamics of high amplitude beta bursts in human motor cortex. *Neuroimage* 242, 118479.
- Brown, P., Oliviero, A., Mazzone, P., Insola, A., Tonali, P., Di Lazzaro, V., 2001. Dopamine dependency of oscillations between subthalamic nucleus and pallidum in Parkinson's disease. *J. Neurosci.* 21, 1033–1038.
- Cagnan, H., Mallet, N., Moll, C.K.E., Gulberti, A., Holt, A.B., Westphal, M., Gerloff, C., Engel, A.K., Hamel, W., Magill, P.J., Brown, P., Sharott, A., 2019. Temporal evolution of beta bursts in the parkinsonian cortical and basal ganglia network. *Proc. Natl. Acad. Sci. USA* 201819975.
- Chen, G., Zhang, Y., Li, X., Zhao, X., Ye, Q., Lin, Y., Tao, H.W., Rasch, M.J., Zhang, X., 2017. Distinct inhibitory circuits orchestrate cortical beta and gamma band oscillations. *Neuron* 96 (1403–1418), e6.
- Confais, J., Malfait, N., Brochier, T., Riehle, A., Kilavik, B.E., 2020. Is there an intrinsic relationship between LFP beta oscillation amplitude and firing rate of individual neurons in macaque motor cortex? *Cereb. Cortex Commun.* 1.
- Deco, G., Jirsa, V., McIntosh, A.R., Sporns, O., Kötter, R., 2009. Key role of coupling, delay, and noise in resting brain fluctuations. *Proc. Natl. Acad. Sci. USA* 106, 10302–10307.
- Deffains, M., Iskhakova, L., Katabi, S., Israel, Z., Bergman, H., 2018. Longer β oscillatory episodes reliably identify pathological subthalamic activity in Parkinsonism. *Mov. Disord.* 33, 1609–1618.
- Diesburg, D.A., Greenlee, J.D.W., Wessel, J.R., 2021. Cortico-subcortical β burst dynamics underlying movement cancellation in humans. *eLife* 10.
- Dietrich, C.R., Newsam, G.N., 1993. A fast and exact method for multidimensional gaussian stochastic simulations. *Water Resour. Res.* 29, 2861–2869.
- Duchet, B., Ghezzi, F., Weerasinghe, G., Tinkhauser, G., Kühn, A.A., Brown, P., Bick, C., Bogacz, R., 2021. Average beta burst duration profiles provide a signature of dynamical changes between the on and off medication states in Parkinson's disease. *PLOS Comput. Biol.* 17, e1009116.
- Enz, N., Ruddy, K.L., Rueda-Delgado, L.M., Whelan, R., 2021. Volume of β -bursts, but not their rate, predicts successful response inhibition. *J. Neurosci.* 41, 5069–5079.
- Feingold, J., Gibson, D.J., DePasquale, B., Graybiel, A.M., 2015. Bursts of beta oscillation differentiate postperformance activity in the striatum and motor cortex of monkeys performing movement tasks. *Proc. Natl. Acad. Sci. USA* 112, 13687–13692.
- Fingelkurts, A.A., Fingelkurts, A.A., 2010. Short-term EEG spectral pattern as a single event in EEG phenomenology. *Open Neuroimaging J.* 4, 130–156.
- Freeman, W.J., 2004. Origin, structure, and role of background EEG activity. Part 1. Analytic amplitude. *Clin. Neurophysiol.* 115, 2077–2088.
- Friston, K.J., 1997. Transients, metastability, and neuronal dynamics. *Neuroimage* 5, 164–171.
- Gerstner, W., Kistler, W.M., Naud, R., Paninski, L., 2014. Neuronal populations. *Neuronal Dynamics: From Single Neurons to Networks and Models of Cognition*. Cambridge University Press, pp. 291–324.
- Halliday, D., Rosenberg, J.R., Amjad, A., Breeze, P., Conway, B.A., Farmer, S.F., 1995. A framework for the analysis of mixed time series/point process data – theory and

- application to the study of physiological tremor, single motor unit discharges and electromyograms. *Prog. Biophys. Mol. Biol.* 64, 237–278.
- Hannah, R., Muralidharan, V., Sundby, K.K., Aron, A.R., 2020. Temporally-precise disruption of prefrontal cortex informed by the timing of beta bursts impairs human action-stopping. *Neuroimage* 222, 117222.
- Heideman, S.G., Quinn, A.J., Woolrich, M.W., van Ede, F., Nobre, A.C., 2020. Dissecting beta-state changes during timed movement preparation in Parkinson's disease. *Prog. Neurobiol.* 184, 101731.
- Inagaki, H.K., Chen, S., Ridder, M.C., Sah, P., Li, N., Yang, Z., Hasanbegovic, H., Gao, Z., Gerfen, C.R., Svoboda, K., 2022. A midbrain-thalamus-cortex circuit reorganizes cortical dynamics to initiate movement. *Cell* 185, 1065–1081 e23.
- Jafarian, A., Zeidman, P., Wykes, R.C., Walker, M., Friston, K.J., 2021. Adiabatic dynamic causal modelling. *Neuroimage* 238, 118243.
- Jansen, B.H., Rit, V.G., 1995. Electroencephalogram and visual evoked potential generation in a mathematical model of coupled cortical columns. *Biol. Cybern.* 73, 357–366.
- Jelfs, B., Javidi, S., Vayanos, P., Mandic, D., 2010. Characterisation of signal modality: exploiting signal nonlinearity in machine learning and signal processing. *J. Signal Process. Syst.* 105–115.
- Jensen, O., Goel, P., Kopell, N., Pohja, M., Hari, R., Ermentrout, B., 2005. On the human sensorimotor-cortex beta rhythm: sources and modeling. *Neuroimage* 26, 347–355.
- Jha, A., Nachev, P., Barnes, G., Husain, M., Brown, P., Litvak, V., 2015. The frontal control of stopping. *Cereb. Cortex* 25, 4392–4406.
- Jones, S.R., 2016. When brain rhythms aren't 'rhythmic': implication for their mechanisms and meaning. *Curr. Opin. Neurobiol.* 72–80.
- Jones, S.R., Pritchett, D.L., Sikora, M.A., Stufflebeam, S.M., Hämäläinen, M., Moore, C.I., 2009. Quantitative analysis and biophysically realistic neural modeling of the MEG mu rhythm: rhythmodgenesis and modulation of sensory-evoked responses. *J. Neurophysiol.* 102, 3554–3572.
- Kanta, V., Pare, D., Headley, D.B., 2019. Closed-loop control of gamma oscillations in the amygdala demonstrates their role in spatial memory consolidation. *Nat. Commun.* 10, 1–14.
- Karvat, G., Alyahyay, M., Diester, I., 2021. Spontaneous activity competes with externally evoked responses in sensory cortex. *Proc. Natl. Acad. Sci. USA* 118.
- Keitel, A., Gross, J., 2016. Individual human brain areas can be identified from their characteristic spectral activation fingerprints. *PLOS Biol.* 14, e1002498.
- Khanna, P., Carmenta, J.M., 2017. Beta band oscillations in motor cortex reflect neural population signals that delay movement onset. *eLife* 6.
- Khawaldeh, S., Tinkhauser, G., Shah, S.A., Peterman, K., Debove, I., Khoa Nguyen, T.A., Nowacki, A., Lenard Lachenmayer, M., Schuepbach, M., Pollo, C., Krack, P., Woolrich, M., Brown, P., 2020. Subthalamic nucleus activity dynamics and limb movement prediction in Parkinson's disease. *Brain* 143, 582–586.
- Kirchgeßner, M.A., Franklin, A.D., Callaway, E.M., 2020. Context-dependent and dynamic functional influence of corticothalamic pathways to first- and higher-order visual thalamus. *Proc. Natl. Acad. Sci. USA* 117, 13066–13077.
- Knudsen, E.B., Wallis, J.D., 2020. Closed-loop theta stimulation in the orbitofrontal cortex prevents reward-based learning. *Neuron* 106, 537–547.
- Kopell, N., Whittington, M.A., Kramer, M.A., 2011. Neuronal assembly dynamics in the beta1 frequency range permits short-term memory. *Proc. Natl. Acad. Sci. USA* 108, 3779–3784.
- Lea-Carnall, C.A., Montemurro, M.A., Trujillo-Barreto, N.J., Parkes, L.M., El-Deredy, W., 2016. Cortical resonance frequencies emerge from network size and connectivity. *PLOS Comput. Biol.* 12, e1004740.
- Lee, J.H., Whittington, M.A., Kopell, N.J., 2013. Top-down beta rhythms support selective attention via interlaminar interaction: a model. *PLOS Comput. Biol.* 9, 1003164.
- Little, S., Bonaiuto, J., Barnes, G., Bestmann, S., 2019. Human motor cortical beta bursts relate to movement planning and response errors. *PLOS Biol.* 17, e3000479.
- Little, S., Beudel, M., Zrinzo, L., Foltynie, T., Limousin, P., Hariz, M., Neal, S., Cheeran, B., Cagnan, H., Gratwicke, J., Aziz, T.Z., Pogosyan, A., Brown, P., 2016. Bilateral adaptive deep brain stimulation is effective in Parkinson's disease. *J. Neurol. Neurosurg. Psychiatry* 87, 717–721.
- Lofredi, R., Tan, H., Neumann, W.J., Yeh, C.H., Schneider, G.H., Kühn, A.A., Brown, P., 2019. Beta bursts during continuous movements accompany the velocity decrement in Parkinson's disease patients. *Neurobiol. Dis.* 127, 462–471.
- Lundqvist, M., Rose, J., Herman, P., Brincat, S.L., Buschman, T.J., Miller, E.K., 2016. Gamma and beta bursts underlie working memory. *Neuron* 90, 152–164.
- Mahjoory, K., Schoffelen, J.M., Keitel, A., Gross, J., 2020. The frequency gradient of human resting-state brain oscillations follows cortical hierarchies. *eLife* 9, 1–18.
- Miller, K.J., 2019. A library of human electrocorticographic data and analyses. *Nat. Hum. Behav.* 3, 1225–1235.
- Miller, K.J., Schalk, G., Fetz, E.E., Den Nijs, M., Ojemann, J.G., Rao, R.P.N., 2010. Cortical activity during motor execution, motor imagery, and imagery-based online feedback. *Proc. Natl. Acad. Sci. USA* 107, 4430–4435.
- Miller, K.J., Leuthardt, E.C., Schalk, G., Rao, R.P.N., Anderson, N.R., Moran, D.W., Miller, J.W., Ojemann, J.G., 2007. Spectral changes in cortical surface potentials during motor movement. *J. Neurosci.* 27, 2424–2432.
- Miller, K.J., Hermes, D., Honey, C.J., Hebb, A.O., Ramsey, N.F., Knight, R.T., Ojemann, J.G., Fetz, E.E., 2012. Human motor cortical activity is selectively phase-entrained on underlying rhythms. *PLOS Comput. Biol.* 8, e1002655.
- Mirzaei, A., Kumar, A., Leventhal, D., Mallet, N., Aertsen, A., Berke, J., Schmidt, R., 2017. Sensorimotor processing in the basal ganglia leads to transient beta oscillations during behavior. *J. Neurosci.* 37, 11220–11232.
- Murthy, V.N., Fetz, E.E., 1996a. Synchronization of neurons during local field potential oscillations in sensorimotor cortex of awake monkeys. *J. Neurophysiol.* 76.
- Murthy, V.N., Fetz, E.E., 1996b. Oscillatory activity in sensorimotor cortex of awake monkeys: synchronization of local field potentials and relation to behavior. *J. Neurophysiol.* 76.
- Oswal, A., Cao, C., Yeh, C.H., Neumann, W.J., Gratwicke, J., Akram, H., Horn, A., Li, D., Zhan, S., Zhang, C., Wang, Q., Zrinzo, L., Foltynie, T., Limousin, P., Bogacz, R., Sun, B., Husain, M., Brown, P., Litvak, V., 2021. Neural signatures of hyperdirect pathway activity in Parkinson's disease. *Nat. Commun.* 12, 1–14.
- Pauls, K.A.M., Korsun, O., Nenonen, J., Nurminen, J., Liljeström, M., Kujala, J., Pekkonen, E., Renvall, H., 2022. Cortical beta burst dynamics are altered in Parkinson's disease but normalized by deep brain stimulation. *Neuroimage* 119308.
- Pavlidis, A., Hogan, S.J., Bogacz, R., 2015. Computational models describing possible mechanisms for generation of excessive beta oscillations in Parkinson's disease. *PLOS Comput. Biol.* 11, e1004609.
- Peles, O., Werner-Reiss, U., Bergman, H., Israel, Z., Vaadia, E., 2020. Phase-specific microstimulation differentially modulates beta oscillations and affects behavior. *Cell Rep.* 30, 2555–2566 e3.
- Pfurtscheller, G., Neuper, C., 1997. Motor imagery activates primary sensorimotor area in humans. *Neurosci. Lett.* 239, 65–68.
- Pfurtscheller, G., Lopes da Silva, F.H., 1999. Event-related EEG/MEG synchronization and desynchronization: basic principles. *Clin. Neurophysiol.* 110, 1842–1857.
- Powanwe, A.S., Longtin, A., 2019. Determinants of brain rhythm burst statistics. *Sci. Rep.* 9, 1–23.
- Reis, C., Sharott, A., Magill, P.J., van Wijk, B.C.M., Parr, T., Zeidman, P., Friston, K.J., Cagnan, H., 2019. Thalamocortical dynamics underlying spontaneous transitions in beta power in Parkinsonism. *Neuroimage* 193, 103–114.
- Rosch, R.E., Hunter, P.R., Baldeweg, T., Friston, K.J., Meyer, M.P., 2018. Calcium imaging and dynamic causal modelling reveal brain-wide changes in effective connectivity and synaptic dynamics during epileptic seizures. *PLOS Comput. Biol.* 14, e1006375.
- Rule, M.E., Vargas-Irwin, C.E., Donoghue, J.P., Truccolo, W., 2017. Dissociation between sustained single-neuron spiking and transient β -LPF oscillations in primate motor cortex. *J. Neurophysiol.* 117, 1524–1543.
- Schalk, G., McFarland, D.J., Hinterberger, T., Birbaumer, N., Wolpaw, J.R., 2004. BCI2000: a general-purpose brain-computer interface (BCI) system. *IEEE Trans. Biomed. Eng.* 51, 1034–1043.
- Schmidt, S.L., Peters, J.J., Turner, D.A., Grill, W.M., 2020. Continuous deep brain stimulation of the subthalamic nucleus may not modulate beta bursts in patients with Parkinson's disease. *Brain Stimul.* 13, 433–443.
- Schnitzler, A., Gross, J., 2005. Normal and pathological oscillatory communication in the brain. *Nat. Rev. Neurosci.* 6, 285–296.
- Schreiber, T., Schmitz, A., 1996. Improved surrogate data for nonlinearity tests. *Phys. Rev. Lett.* 77, 635–638.
- Seedat, Z.A., Quinn, A.J., Vidaurre, D., Liuzzi, L., Gascoyne, L.E., Hunt, B.A.E., O'Neill, G.C., Pakenham, D.O., Mullinger, K.J., Morris, P.G., Woolrich, M.W., Brookes, M.J., 2020. The role of transient spectral 'bursts' in functional connectivity: a magnetoencephalography study. *Neuroimage* 209, 116537.
- Sherman, M.A., Lee, S., Law, R., Haegens, S., Thorn, C.A., Hämäläinen, M.S., Moore, C.I., Jones, S.R., 2016. Neural mechanisms of transient neocortical beta rhythms: converging evidence from humans, computational modeling, monkeys, and mice. *Proc. Natl. Acad. Sci. USA* 113, E4885–E4894.
- Shin, H., Law, R., Tsutsui, S., Moore, C.I., Jones, S.R., 2017. The rate of transient beta frequency events predicts behavior across tasks and species. *eLife* 6.
- Siegel, M., Donner, T.H., Engel, A.K., 2012. Spectral fingerprints of large-scale neuronal interactions. *Nat. Rev. Neurosci.* 12, 121–134.
- Takeuchi, D., Hirabayashi, T., Tamura, K., Miyashita, Y., 2011. Reversal of interlaminar signal between sensory and memory processing in monkey temporal cortex. *Science* 331, 1443–1447.
- Theiler, J., Eubank, S., Longtin, A., Galdrikian, B., Doynne Farmer, J., 1992. Testing for nonlinearity in time series: the method of surrogate data. *Phys. D. Nonlinear Phenom.* 58, 77–94.
- Tinkhauser, G., Pogosyan, A., Tan, H., Herz, D.M., Kühn, A.A., Brown, P., 2017b. Beta burst dynamics in Parkinson's disease OFF and ON dopaminergic medication. *Brain* 140, 2968–2981.
- Tinkhauser, G., Pogosyan, A., Little, S., Beudel, M., Herz, D.M., Tan, H., Brown, P., 2017a. The modulatory effect of adaptive deep brain stimulation on beta bursts in Parkinson's disease. *Brain* 140, 1053–1067.
- Toni, T., Welch, D., Strelkowa, N., Ipsen, A., Stumpf, M.P., 2009. Approximate Bayesian computation scheme for parameter inference and model selection in dynamical systems. *J. R. Soc. Interface* 6, 187–202.
- Torrecllos, F., Tinkhauser, G., Fischer, P., Green, A.L., Aziz, T.Z., Foltynie, T., Limousin, P., Zrinzo, L., Ashkan, K., Brown, P., Tan, H., 2018. Modulation of Beta bursts in the subthalamic nucleus predicts motor performance. *J. Neurosci.* 38, 8905–8917.
- Tzagarakis, C., Ince, N.F., Leuthold, A.C., Pellizzer, G., 2010. Beta-band activity during motor planning reflects response uncertainty. *J. Neurosci.* 30, 11270–11277.
- van Ede, F., Quinn, A.J., Woolrich, M.W., Nobre, A.C., 2018. Neural oscillations: sustained rhythms or transient burst-events? *Trends Neurosci.* 41, 415–417.
- Van Rheede, J.J., Feldmann, L.K., Busch, J.L., Fleming, J.E., Mathiopoulos, V., Denison, T., Sharott, A., Kühn, A.A., 2022. Diurnal modulation of subthalamic beta oscillatory power in Parkinson's disease patients during deep brain stimulation. *medRxiv*, 02.09.22270606, 2022.
- Veit, J., Hakim, R., Jädi, M.P., Sejnowski, T.J., Adesnik, H., 2017. Cortical gamma band synchronization through somatostatin interneurons. *Nat. Neurosci.* 20, 951–959.
- Vogels, T.P., Abbott, L.F., 2009. Gating multiple signals through detailed balance of excitation and inhibition in spiking networks. *Nat. Neurosci.* 12, 483–491.

- Vogels, T.P., Rajan, K., Abbott, L.F., 2005. Neural network dynamics. *Annu Rev. Neurosci.* 28, 357–376.
- Wessel, J.R., 2020. β -bursts reveal the trial-to-trial dynamics of movement initiation and cancellation. *J. Neurosci.* 40, 411–423.
- West, T.O., Berthouze, L., Farmer, S.F., Cagnan, H., Litvak, V., 2021. Inference of brain networks with approximate Bayesian computation – assessing face validity with an example application in Parkinsonism. *Neuroimage* 118020.
- West, T.O., Magill, P.J., Sharott, A., Litvak, V., Farmer, S.F., Cagnan, H., 2022. Stimulating at the right time to recover network states in a model of the cortico-basal ganglia-thalamic circuit. *PLOS Comput. Biol.* 18, e1009887.
- Wilson, H.R., Cowan, J.D., 1972. Excitatory and inhibitory interactions in localized populations of model neurons. *Biophys. J.* 12, 1–24.
- Wilson, H.R., Cowan, J.D., 1973. A mathematical theory of the functional dynamics of cortical and thalamic nervous tissue. *Kybernetik* 13, 55–80.
- Xing, D., Shen, Y., Burns, S., Yeh, C.I., Shapley, R., Li, W., 2012. Stochastic generation of gamma-band activity in primary visual cortex of awake and anesthetized monkeys. *J. Neurosci.* 32, 13873–13880.
- Yamawaki, N., Borges, K., Suter, B.A., Harris, K.D., Shepherd, G.M.G., 2014. A genuine layer 4 in motor cortex with prototypical synaptic circuit connectivity. *eLife* 3.
- Yousif, N., Mace, M., Pavese, N., Borisyuk, R., Nandi, D., Bain, P., 2017. A network model of local field potential activity in essential tremor and the impact of deep brain stimulation. *PLOS Comput. Biol.* 13.
- Zich, C., Quinn, A.J., Mardell, L.C., Ward, N.S., Bestmann, S., 2020. Dissecting transient burst events. *Trends Cogn. Sci.* 784–788.